FUEL CELL PRESSURE LOADING DURING HYDRAULIC RAM

John W. Patterson

NAVAL POSTGRADUATE SCHOOL
Monterey, California

THESIS

FUEL CELL PRESSURE LOADING
DURING HYDRAULIC RAM

by

John W. Patterson

June 1975

Thesis Advisor: H. L. Power, Jr.

SECURITY CLASSIFICATION OF THIS PAGE (When Data Entered)

REPORT DOCUMENTATION PAGE

READ INSTRUCTIONS BEFORE COMPLETING FORM

1. REPORT NUMBER	2. GOVT ACCESSION NO. / 3. RECIPIENT'S CATALOG NUMBER
4. TITLE (and Subtitle): Fuel Cell Pressure Loading During Hydraulic Ram	5. TYPE OF REPORT & PERIOD COVERED: Master's Thesis, June 1975
	6. PERFORMING ORG. REPORT NUMBER
7. AUTHOR(s): John W. Patterson	8. CONTRACT OR GRANT NUMBER(s)
9. PERFORMING ORGANIZATION NAME AND ADDRESS: Naval Postgraduate School, Monterey, California 93940	10. PROGRAM ELEMENT, PROJECT, TASK AREA & WORK UNIT NUMBERS
11. CONTROLLING OFFICE NAME AND ADDRESS: Naval Postgraduate School, Monterey, California 93940	12. REPORT DATE: June 1975
	13. NUMBER OF PAGES: 61
14. MONITORING AGENCY NAME & ADDRESS (if different from Controlling Office): Naval Postgraduate School, Monterey, California 93940	15. SECURITY CLASS. (of this report): Unclassified
	15a. DECLASSIFICATION/DOWNGRADING SCHEDULE

16. DISTRIBUTION STATEMENT (of this Report)

Approved for public release, distribution unlimited.

17. DISTRIBUTION STATEMENT (of the abstract entered in Block 20, if different from Report)

18. SUPPLEMENTARY NOTES

19. KEY WORDS (Continue on reverse side if necessary and identify by block number)

20. ABSTRACT (Continue on reverse side if necessary and identify by block number)

Hydraulic ram is the phenomenon associated with the damage caused by high speed projectile impacts with fuel tanks. It is divided into five phases, entry, shock, drag, cavity and exit. The entry, shock and drag phases were of concern in this study.

An analytical solution for the pressures developed in the shock phase was formulated based on bullet impact parameters.

Pressures developed in the drag phase were experimentally

correlated with theoretical predictions. These pressures were proven to be dependent on front wall wave reflections.

Fuel Cell Pressure Loading During Hydraulic Ram

by

John W. Patterson
Lieutenant Commander, United States Navy
B.S., Naval Postgraduate School, 1964
M.S.I.R., George Washington University, 1971

Submitted in partial fulfillment of the
requirements for the degree of

MASTER OF SCIENCE IN AERONAUTICAL ENGINEERING

from the

NAVAL POSTGRADUATE SCHOOL
June 1975

ABSTRACT

Hydraulic ram is the phenomenon associated with the damage caused by high speed projectile impacts with fuel tanks. It is divided into five phases, entry, shock, drag, cavity and exit. The entry, shock and drag phases were of concern in this study.

An analytical solution for the pressures developed in the shock phase was formulated based on bullet impact parameters.

Pressures developed in the drag phase were experimentally correlated with theoretical predictions. These pressures were proven to be dependent on front wall wave reflections.

TABLE OF CONTENTS

LIST OF FIGURES

LIST OF SYMBOLS

A	Cross sectional area of deformed projectile
B	Velocity decay coefficient defined by equation (II-3)
C	Speed of sound in undisturbed fluid
C_D	Drag coefficient
E	Projectile kinetic energy
E_B	Projectile kinetic energy at ballistic limit
E_C	Projectile kinetic energy at impact
E_0	Projectile kinetic energy released at point source
m	Projectile mass
m_p	Mass per unit area of wall
R_0	Initial Radius defined by equation (II-2)
R_s	Shock Radius
T	Thickness of wall
t	Time
V	Projectile velocity
V_i	Projectile impact velocity
ΔV_s	Change in projectile velocity
X	Distance coordinate
α	Measure of wall rigidity, defined by equation (IV-1)
θ	Time constant of an exponential pressure wave
ρ_o	Density of the undisturbed fluid
σ_y	Dynamic yield strength of wall material

ACKNOWLEDGEMENTS

The cooperation and assistance of Ted Dunton, Glenn Middleton and the other members of the Department of Aeronautics Technical Staff, without whose help this study would not have been possible, are gratefully acknowledged. Special acknowledgement is made to Professor Power for his assistance, cooperation and patience.

I. INTRODUCTION

The study of aircraft survivability has become increasingly important in recent years. This increase in importance is due to several factors. Among these are the escalating cost and concomitant complexity of modern aircraft making the loss of an aircraft less acceptable. The increased complexity of modern aircraft also tends to make them more vulnerable to anti-aircraft weapons. At the same time anti-aircraft defensive capability is increasing; witness the widespread introduction of hand held infrared guided missiles of the Redeye class. These factors make survivability analysis and design of economic and military importance. One of the most promising areas for survivability analysis is the fuel system; in particular fuel cells. This is because the fuel cells occupy a large percentage of the total volume of the aircraft and are therefore most susceptible to damage. Damage to the fuel cell can result in fuel starvation, structural damage, fires or explosion; any of which can result in the loss of an aircraft.

The interaction of the projectile and the fluid in the fuel cell produces damage that is many times greater than that caused by impact with an empty cell. One of the mechanisms that can cause damage is fire and/or explosion of the fluid. Hydraulic ram refers to the complicated dynamic interaction of the projectile, cell walls and the

fuel. These interactions produce internal pressure pulses which load the fuel cell structural members and produce damage.

Hydraulic ram is usually divided into several phases that are associated with different major pressure pulse characteristics that occur during the passage of the projectile through the fluid. The five phases of hydraulic ram are the entry, shock, drag, exit and cavity phases. The entry and exit phases occur when the projectile penetrates the respective fuel cell walls. The shock phase is associated with the initial transfer of the projectile kinetic energy to the fluid in the cell. This energy transfer creates a strong shock wave. The drag phase occurs as the projectile continues through the fluid and transfers more energy to the fluid through viscous dissipation and pressure drag. The cavity phase occurs as the cavity, which was created in the drag phase, overexpands, is compressed, rebounds and continues to oscillate until the energy is dissipated. The entry, shock and drag phases will always occur in order. The exit phase may not occur, and it may precede or overlap the cavity phase depending on the size of the tank, projectile impact velocity and other factors. Hydraulic ram research has been conducted by various investigators. This study was designed to extend Yurkovich's [Ref. 1] analytical solution for the shock phase fuel cell

pressure loadings and to verify experimentally the analytical solution of drag phase pressures of Lundstrom [Ref. 2].

II. DESCRIPTION OF HYDRAULIC RAM PHENOMENON

In analyzing hydraulic ram all five phases must be considered. The damage associated with hydraulic ram is dependent upon the anti-aircraft threat and the physical characteristics of the fuel cell. The threat determines the path, energy level and size of impacting projectiles. The fuel cell size, geometry, location and construction, in conjunction with the threat, determines the dominant phase of the hydraulic ram phenomenon. For example, there may not be an exit phase for a low energy threat impacting a tank with sufficiently large dimensions along the projectile path.

In any phase of hydraulic ram the damage is related to the energy dissipated in that phase. This makes the determination of the energy loss during the entry phase (wall penetration) essential. The energy dissipated during the entry phase is a function of wall parameters (thickness, yield strength) and projectile initial energy, obliquity of impact, material properties, and tumbling. Studies by Soper [Ref. 3] have shown that the percentage of energy loss for untumbled, normal entries can be approximated by:

$$\% E_{lost} = \frac{E_i - E_B}{E_i} = \frac{200\ \sigma_y\ AT}{m}\left(\frac{1}{V_i^2}\right) \qquad \text{(II-1)}$$

The studies also have shown that the penetration energy loss is independent of projectile shape. If the projectile has

not tumbled and strikes normal to the wall, the damage area (A) approximately equals the cross sectional area of the projectile.

If the projectile energy is sufficiently high, it will penetrate into the tank fluid and produce a strong hemispherical shock wave centered about the penetration point. This is the start of the shock phase. The shock phase is characterized by high pressures of short duration (microsecs) that are independent of fuel cell geometry. After the bullet enters the fluid, it has little effect on the shock wave strength or shape. Investigations have shown that shock phase pressures generated are a function both of the energy transferred to the fluid at impact and of the fluid properties. The shock wave pressures are attenuated rapidly as the wave is propagated through the fluid. Therefore, the damage associated with the shock phase is generally limited to the entry wall. This damage is caused by the impulsively generated pressure field combined with whatever damage (cracks, etc.) the initial penetration of the wall may have caused.

An analytical formulation of the shock phase problem has been postulated by Yurkovich [Ref. 1]. In this formulation the shock formation process of the shock phase has been modeled as a point energy source release. The formulation assumes that the fuel cell walls are rigid, and that the shock radius is proportional to a constant power of time.

The assumption that the radius is proportional to a constant power of time has been supported by several investigators [Ref. 4, 5, 6].

The Rankine-Hugoniot equations are used to formulate the flow properties at the shock front. A fourth equation is provided by the Tait equation of state for isothermal compressible liquid. The fluid property changes at the shock front are assumed to be adiabatic. If the shock radius is known, a shock Mach number can be computed from energy considerations. From the shock Mach number the shock front pressure and density can then be computed, using the above equations. Reference 2 postulates the initial radius is a function of energy deposited given by:

$$R_0 = \left(\frac{E_0}{\rho_o C^2 2\pi} \right)^{1/3} \qquad \text{(II-2)}$$

where E_0 is the energy released in the shock phase, C is the speed of sound and ρ_o is the density in the undisturbed fluid.

The flow parameters behind the shock front are computed using the unsteady motion, one-dimensional equations, for conservation of mass, energy and momentum, again coupled with the state equation. To use these equations a power law density distribution was assumed. The radial velocity distribution was found by integrating the continuity equation. Integration of the momentum equation then yields the

pressure. Integration of the energy density behind the shock front, knowing the shock Mach number and radius, would then yield the energy released during the shock phase. Since the energy released is assumed to be known, solving the energy integral for the shock Mach number is possible. Once the shock Mach number is known as a function of radius, the shock radius as a function of time can be found by integration. It is then possible to determine the pressure, shock Mach number and radius, as a function of time, anywhere in the field. In this formulation, then, the energy released in the shock phase must be known.

Since, in most cases, not all of the projectile energy has been released during the shock phase, another phenomenon of hydraulic ram becomes important. This phase is referred to as the drag phase. It is distinguished from the shock phase by the gradual acceleration of the fluid vice the impulsive acceleration characteristic of the shock phase. The energy transfer, therefore, is due to viscous dissipation and form drag. Drag is normally characterized by defining a drag coefficient. The drag coefficient of a projectile is not a constant but varies with velocity, shape and tumbling behavior. If the projectile velocity is below the drag divergence Mach number, however, changes in velocity have only a small effect on drag coefficient size. The effect of shape and tumbling is then the dominant variable for estimating the drag coefficient for a

projectile. Experiments [Ref. 2] have indicated that soon after entry (within one foot) the projectiles will begin to tumble. Furthermore, because of the high stagnation pressures on the nose of the bullet, soft nosed projectiles may begin to deform. This phenomenon effectively changes the shape of the projectile and therefore the drag coefficient.

The pressure disturbance in the drag phase is propagated through the fluid at the fluid sonic velocity. Since the energy transfer is more gradual, the peak pressures are lower during this phase. But the pulses are of much longer duration (hundreds of microsecs). During this phase a cavity is formed behind the projectile. The cavity is cylindrical in shape and its size and expansion rate are dependent on the rate of energy dissipation by the projectile.

Lundstrom [Ref. 2] has formulated an analytical solution for the drag phase pressures. In this model a velocity decay factor B is defined as a function of the drag coefficient, mass, area, and density of the fluid:

$$B = \rho_o C_D \, A/2m \qquad \text{(II-3)}$$

Then the rate of energy dissipation with distance is given as:

$$\frac{dE}{dx} = m \, BV^2 \qquad \text{(II-4)}$$

where B is assumed to be independent of velocity. The flow field properties are then solved for by using a potential

function that satisfies the wave equation. A line of sources is distributed along the projectile path with the strength of the sources being determined by an energy balance. The effect of wall restraint on cavity growth is not considered, so that the analysis will not yield useful pressures during cavity collapse.

The pressure wave reflections at the fuel cell boundaries are assumed to be similar to those of a free surface. A system of negative image sources is utilized which result in zero pressure perturbation at the walls. Pressure waves reflected from the cavity surfaces are not considered.

The next phase to be considered is the cavity oscillation phase. This is a complex phase and the least understood. Part of the complexity is due to the many reflected pressure waves that have had time to be of significance. The cavity is formed during the drag phase as the momentum of the fluid becomes large enough to cause the fluid to separate from the projectile surface. A void is created which is filled with fluid vapors and air that enters through the wall penetration point. The cavity then grows until it is arrested by fluid pressures developed by the walls, and collapses. During the collapse the momentum of the fluid causes the entrapped gases and air to be compressed and the cavity begins to expand again. It is this alternating expansion and contraction that produces low amplitude pressure pulses of long duration. The phase continues until all the

energy is absorbed by the fluid. High speed motion pictures [Ref. 7] have shown that the pressure oscillations can lead to eventual catastrophic failure of walls already weakened by the drag and exit phases.

The exit phase will occur if the energy transferred from the projectile during the entry, shock and drag phases has not dissipated all the kinetic energy of the projectile by the time the exit wall is reached. Pressure loadings due to projectile proximity to the wall, and fluid motion produced in the earlier phases, can cause catastrophic damage to the exit wall. If this occurs, the latter phase (cavity oscillation) causes little further damage but does pump fuel from the tank, causing fire hazard.

From the above discussion it is apparent that each of the different phases of hydraulic ram produces damage to the fuel tank in a distinct manner. The entry phase results in a hole in the tank entry wall. The damage from the shock phase is usually limited to the entry wall and can lead to catastrophic failure. The drag phase results in lower pressure amplitudes, but of longer duration, which can cause high levels of stress on all fuel cell walls. The cavity phase has even lower pressure amplitude but longer pulse widths and is oscillating in nature. This can result in damage to the already weakened fuel cell walls. The exit phase causes damage to the exit wall, usually before the cavity phase. It should also be apparent that impact energy

and the physical characteristics of the fuel cell determine which phase is dominant.

III. HYDRAULIC RAM PRESSURE EXPERIMENT

The Naval Postgraduate School Ballistic Range was used to conduct the experimental part of this study. The basic components of the range were a rifle, velocity measuring equipment, simulated fuel tank, and pressure measuring and recording equipment. Figure III-1 is a schematic of the basic components and Figure III-2 is a down range view.

The rifle was a .222 caliber Remington. Cartridges were loaded to obtain the 7,493 in.-lb. energy level with a 45 grain spitzer ogive nose bullet. The velocity of the bullet was measured by using the first three Avtron No. A914T33 chronograph screens to trigger two Monsanto 101B counters. Two counters were used to increase the accuracy of velocity measurements and for redundancy.

The simulated fuel tank was constructed of welded .160-inch 7075-T6 aluminum plate on the sides, back and bottom walls. The front wall was .05-inch 7075-T6 aluminum. A one-inch hole was drilled in the front wall for bullet entry. The hole allowed calculation of precise impact energy. The top of the tank was left open. The side and bottom walls of the tank were welded to a frame of .5-inch thick, three-inch aluminum angle sections for added strength. The entry and exit wall were bolted to the frame. The inside dimension of the tank was 18x18x18-inches. Figure III-3 shows the tank.

A Kistler 603A quartz pressure transducer was used to measure the hydraulic ram pressure pulse at several points

internal to the tank. The transducer was mounted in a hollow 1.0-inch stainless steel tube. The transducer was held in the tube by a nylon ring. The tube was then sealed with RTV. In this manner the transducer and cable were kept dry. The tube had a 45^{o} angle at the tip and was mounted on the tank at 50^{o} from the vertical to obtain pressure measurements along a radial line. Figure III-4 shows the transducer and probe assembly. The probe was then secured to the top of the tank so that it could be positioned for measurements at 2,4,6,8 and 10 inches along a radial line from the impact point.

The charge signal from the pressure transducer was fed into a Kistler Model 504E charge amplifier with a 545A14 filter and displayed on an oscilloscope. A Polaroid camera mounted on the oscilloscope recorded the pressure trace. The oscilloscope was triggered by the fourth chronograph screen mounted one inch in front of the tank wall.

Several firings were made at each distance for consistency and accuracy. Typical results for each distance are shown in Figures III-5, 6, 7.

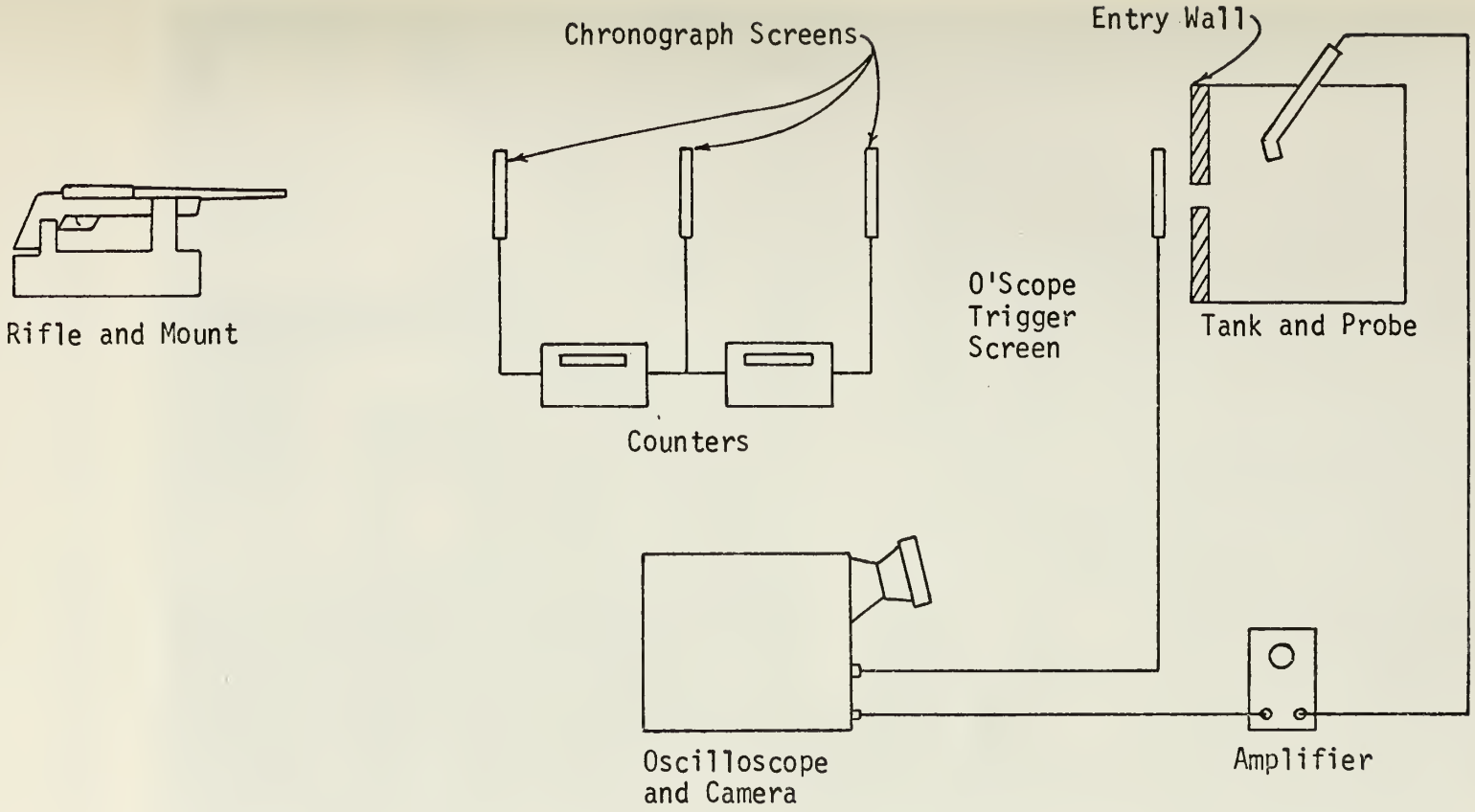

Figure III-1. Ballistic Range Components

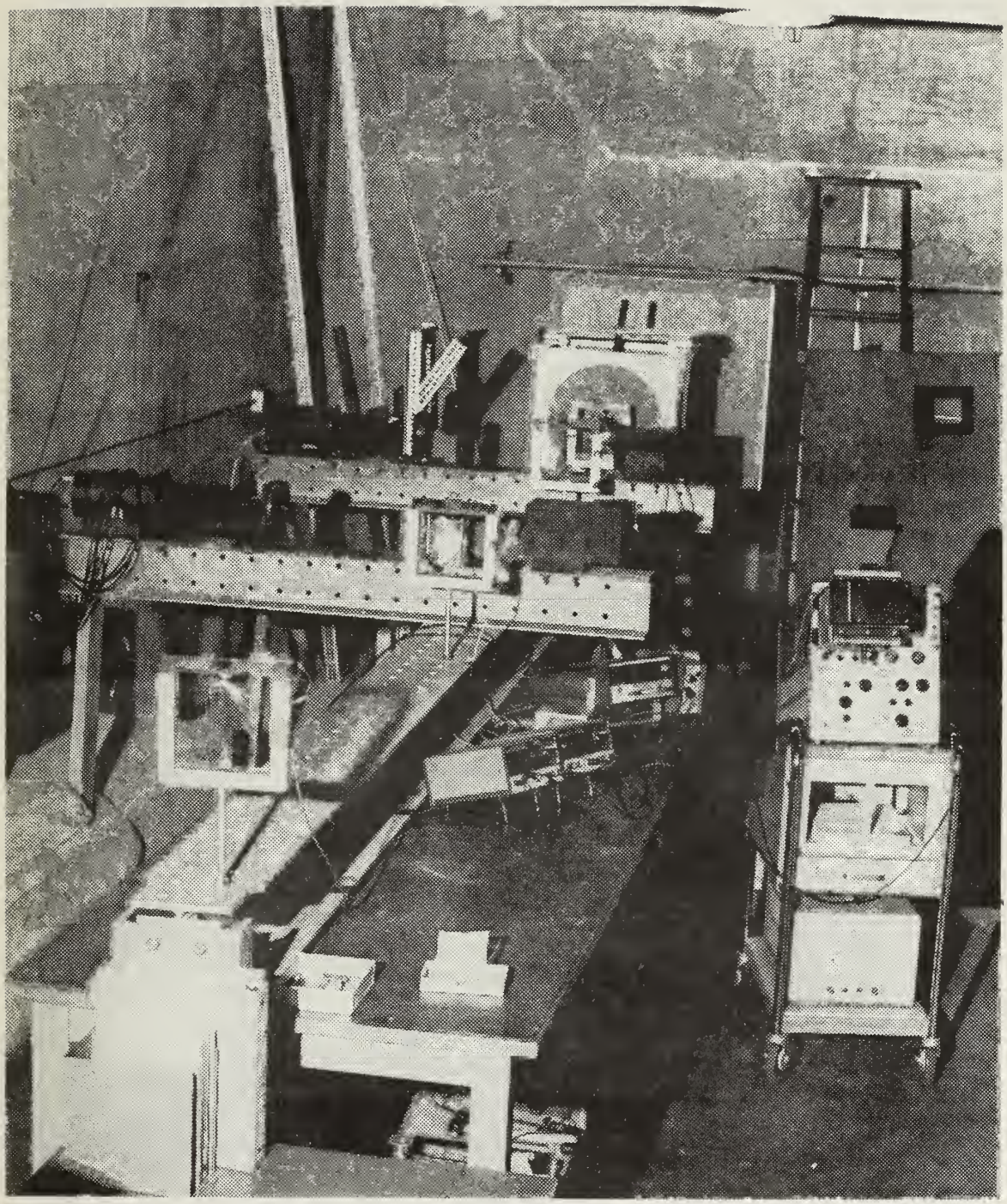

Figure III-2. Ballistic Range.

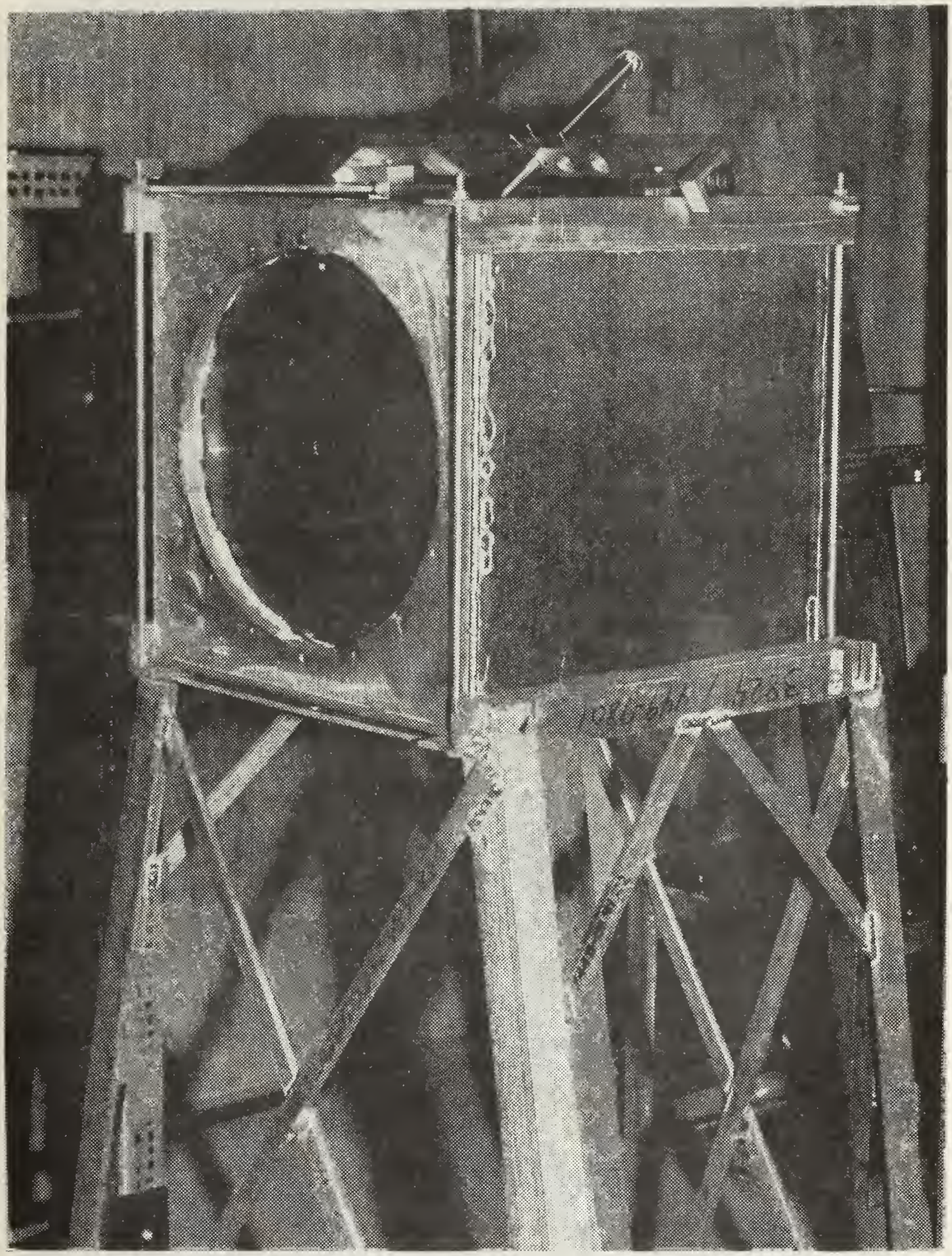

Figure III-3. Fuel Cell and Probe Installation.

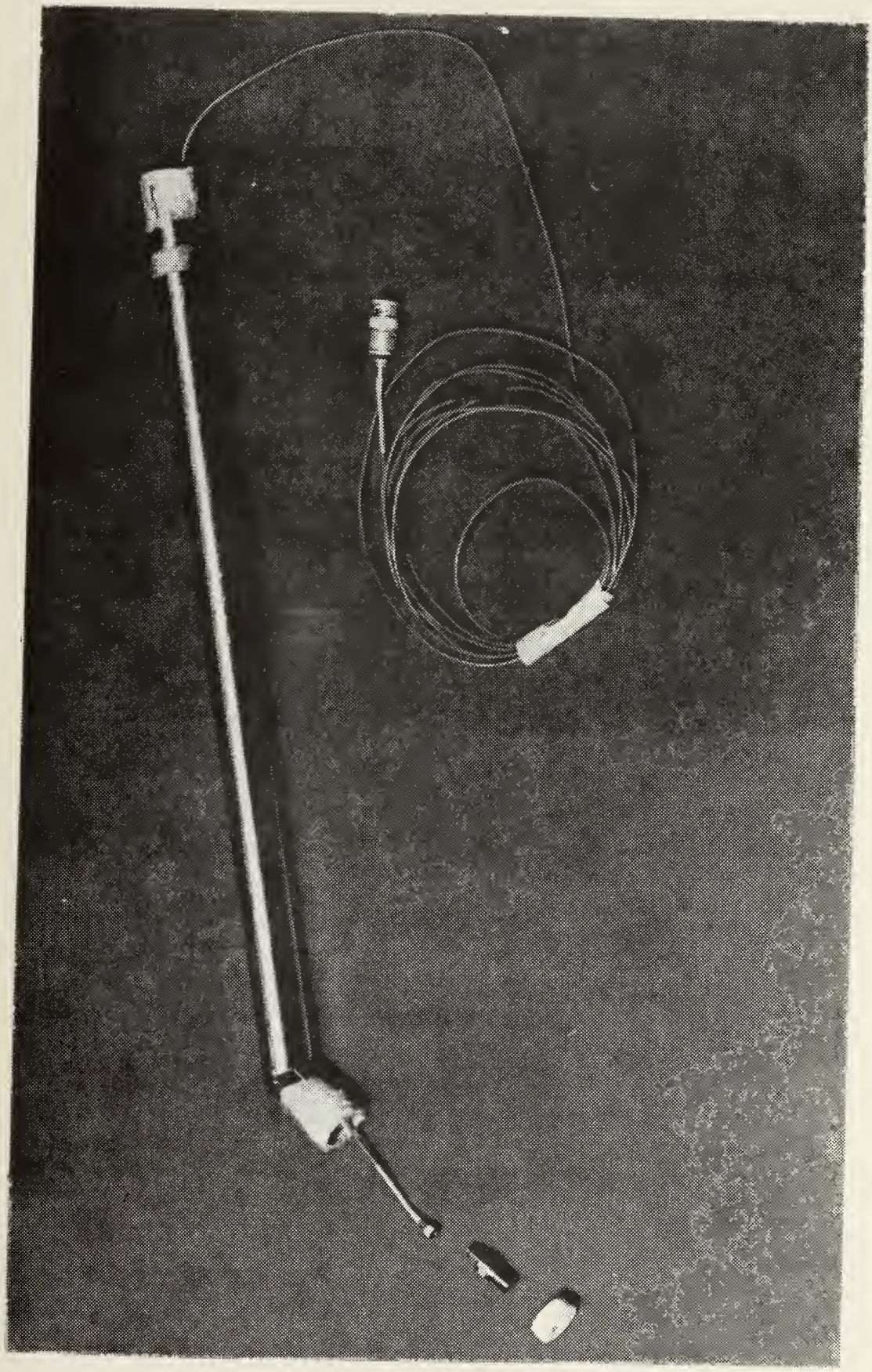

Figure III-4. Disassembled Probe.

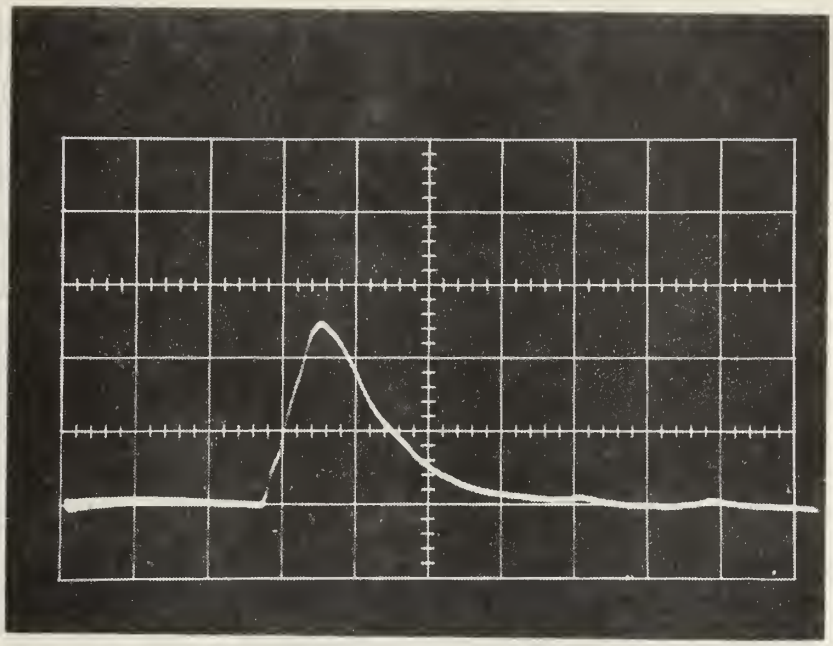

Radius = 2 in
Scale: 1000 psi/cm, 50 microsecs/cm

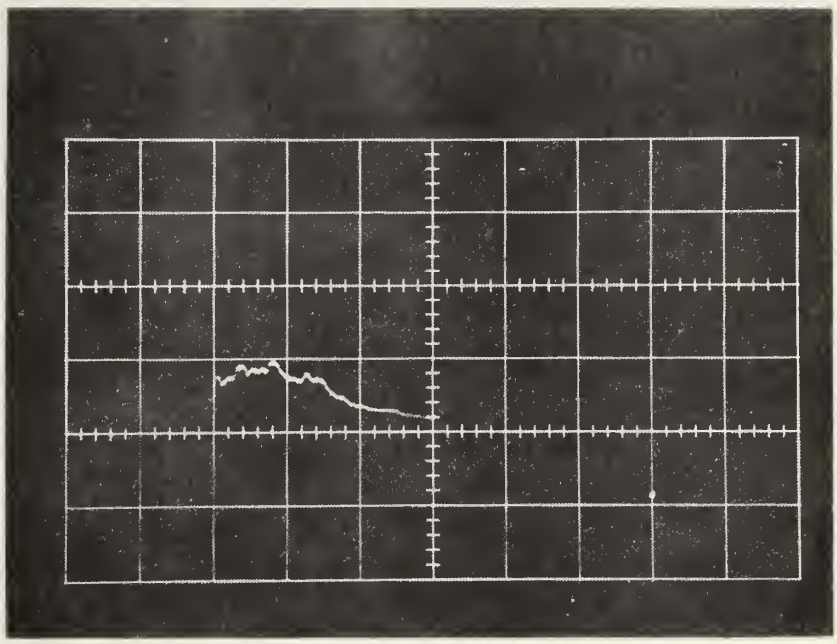

Radius = 4 in
Scale: 500 psi/cm, 50 microsecs/cm

Figure III-5. Pressure vs. Time, E_0 = 7,493 in-lb Light Wall.

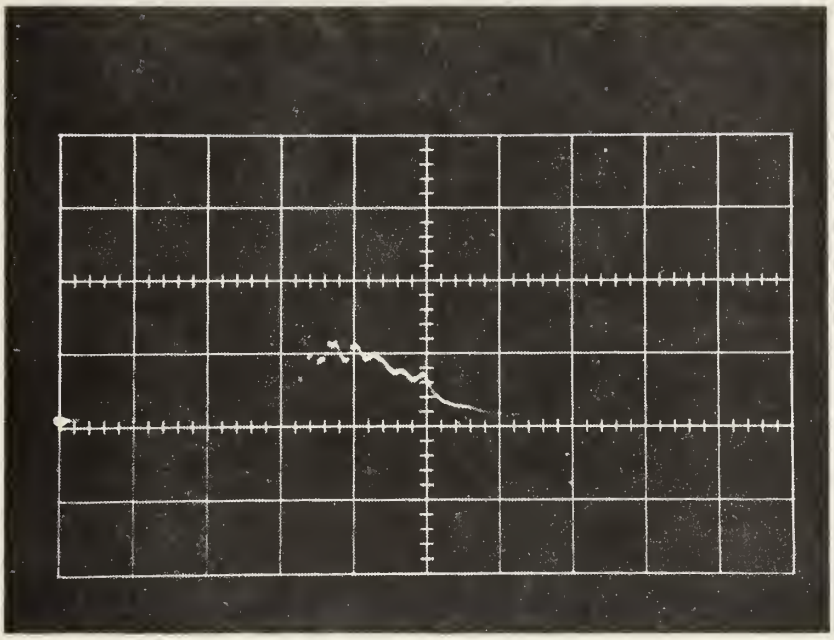

Radius = 6 in

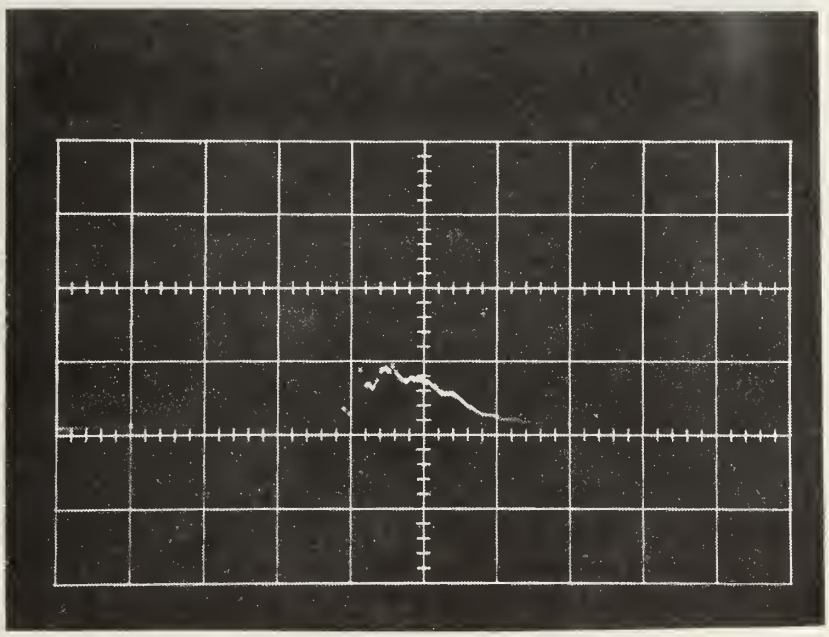

Radius = 8 in

Figure III-6. Pressure vs. Time, E_0 = 7,493 in-lb Light Wall. Scale: 500 PSI/cm, 50 microsecs/cm.

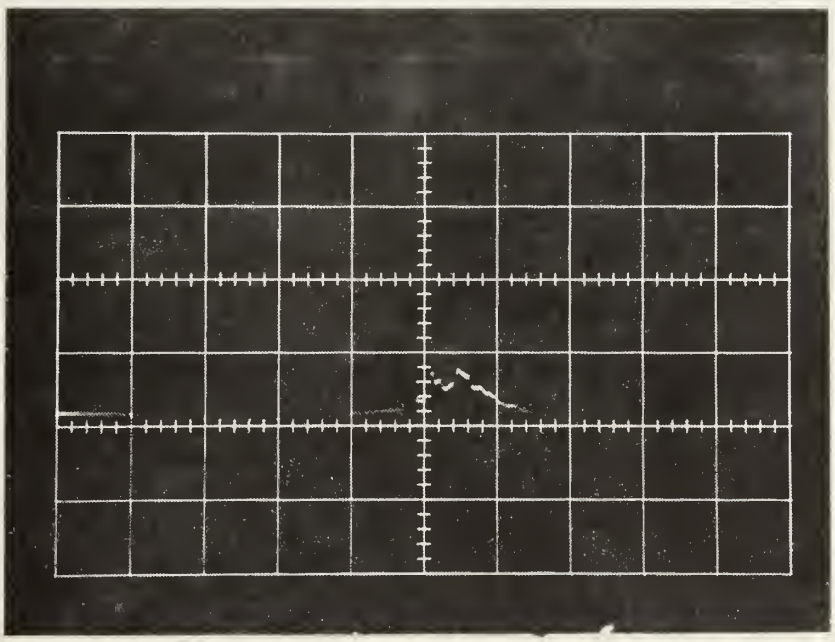

Radius = 10 in

Scale: 500 psi/cm, 50 microsecs/cm.

Figure III-7. Pressure vs. Time, E_0 = 7,493 in-lb Light Wall.

IV. ANALYSIS

The first segment of this study was to improve the computer code for shock phase pressures developed by Kappel [Ref. 4]. This code was based on the formulation of Yurkovich discussed in Section II.

To account for the energy dissipated by the projectile in penetrating the entry wall the formulation of Soper was added to the computer code.

A method for computing the energy deposited during the shock phase was needed as previous formulations assumed this value was known. Studies [Ref. 4, 5] have indicated that the energy released in the shock phase is a constant percentage of the impact energy. This percentage is a function of the impact Mach number with respect to the fluid speed of sound. Plots of experimentally observed changes in projectile velocity during the characteristic shock formation with projectile impact were made by Power [Ref. 8]. This plot is reproduced as Figure IV-1. In addition, the corresponding shock phase energy dissipation percentage of the impact energy is shown. It can be seen that impact Mach number with respect to the tank fluid is critical in determining the shock phase energy input. For Mach numbers less than sonic the input percentage is approximately 10 percent and for moderate supersonic speeds the energy input percentage is greater than 80 percent. This provided an empirical

procedure for determining shock phase energy input as a function of bullet impact parameters.

The shock front pressures are quickly attenuated and become acoustic. Figure IV-2 shows the radius and time for the shock wave to become acoustic versus input energy for both water and fuel. To calculate pressures after the acoustic speed was reached, a simple expression based on acoustic wave theory was used. The shape of the wave was assumed to remain constant and the pressure amplitude varied as the inverse of the radius.

Since the Yurkovich theory postulates the energy release as a point source, the model can be extended to an explosion in the fuel cell. This type of event is characteristic of an H.E. round impact. This was accomplished by integrating the energy equation over a spherical volume. In this case, however, the shock phase energy that is released by the explosion must be known.

Figures IV-3, 4 and 5 show the predicted pressure distribution for .50 caliber, 12.7mm and 14.5mm AP projectiles impacting JP-5 fuel. The plots illustrate the very high pressures generated and their rapid decay. Figures IV-6 through 11 show the predicted shock phase pressure versus time at a constant radius for a .222 caliber projectile impacting water. Also shown in these figures are measured pressures from reference 9 and analytical drag phase pressures to be discussed. From these figures it can be

seen that the shock phase pressures could not be measured. This is due to the very rapid rise time of the shock phase pressures. The pressure transducers and associated measuring equipment were unable to follow the signal. This phenomenon was also reported by Williams [Ref. 10].

Experiments were undertaken to verify the drag phase pressures predicted by Lundstrom. Holm in reference 9 reported that the drag phase pressures could not be verified. In that experiment the front wall of the fuel tank was a heavy, .5-inch, mild steel plate. Lundstrom's formulation of the problem treats the walls as free surfaces. This is done by using a set of negative image sources so that the pressure at the wall is zero.

The degree to which a wall may be considered rigid or free is characterized by the expression [Ref. 2]:

$$\alpha = \rho C \theta / m_p \qquad \text{(IV-1)}$$

where θ is the time constant. A rigid surface corresponds to $\alpha=0$, and a free surface to $\alpha=\infty$. For a .5-inch thick steel plate $\alpha=1.5$, while for a .05-inch thick aluminum plate $=44.5$. The heavy steel plate is then an approximation to a rigid surface while the .05-inch aluminum plate is an approximation to a free surface.

A set of image sources that can approximate the rigid surface would be a positive set. Using this set of positive images on the front wall for the pressures reported in

reference 9 resulted in very close agreement. This is illustrated in Figures IV-6 through 11 for two energy levels. The peak pressure versus radius is depicted in Figure IV-12. Close agreement is shown at medium and larger radii. The theory does underestimate the pressures at small radii however.

The experiment was repeated using a .05-inch aluminum front wall to approximate a free surface. Plots of the pressure distribution versus time at a constant radius are shown in Figures IV-13 and 14. These figures also show close agreement between the experiment and theory when a free surface is assumed.

A plot of peak pressure versus radius compared with theoretical values is shown in Figure IV-15. Again, the theory underestimates the peak pressure for small radii.

All of the theoretical pressures were computed using a drag coefficient of one. This coefficient was determined from the experimental data of reference 3. The theoretical formulation allows a variation of drag coefficient with time. This would account for any tumbling of the projectile. No measurements of the tumbling behavior were possible, so a constant C_D was assumed. Photographs of the bullet trajectory would be required to determine tumbling distances.

The pulse shape discrepancy was due to the assumption that C_D was a constant. If detailed measurements are made, the pulse shape will be more accurately predicted.

Reference 11 reports that a data base was established for the tumbling behavior of 14.5mm and 12.7mm projectiles. From these data good correlation of pressures was possible.

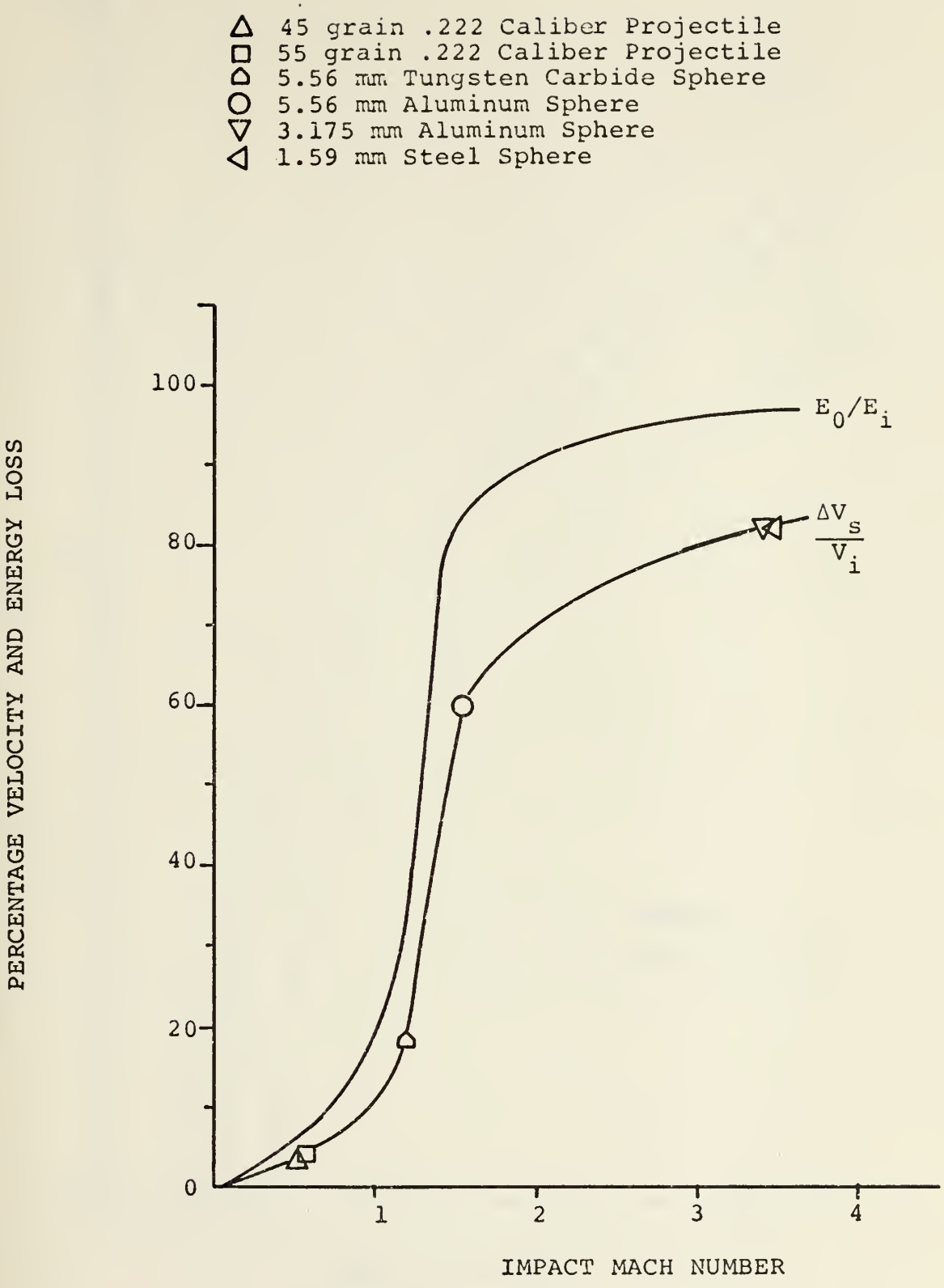

Figure IV-1. Shock Phase Energy Release.

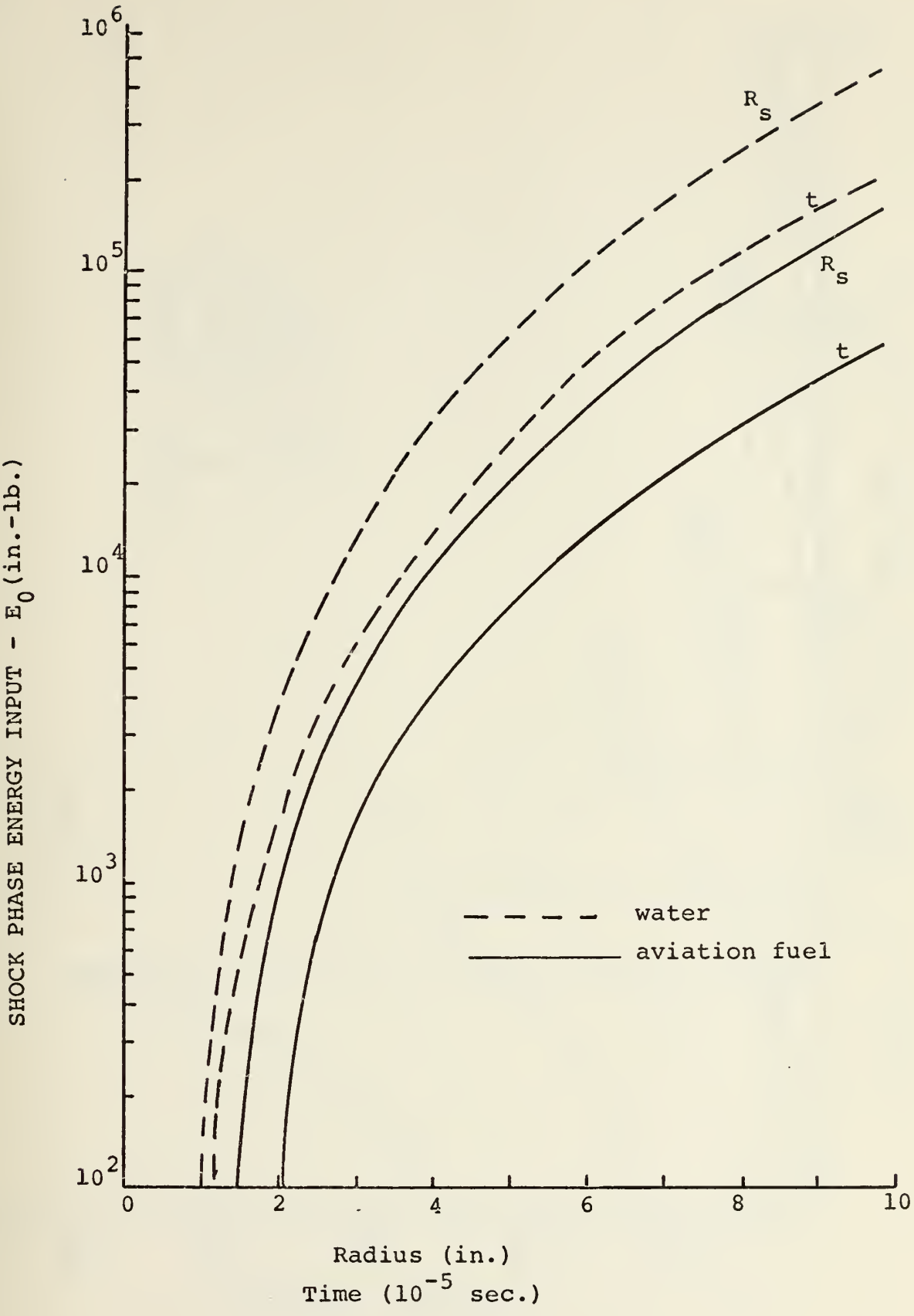

Figure IV-2. Radius and Time for Acoustic Shock Speed.

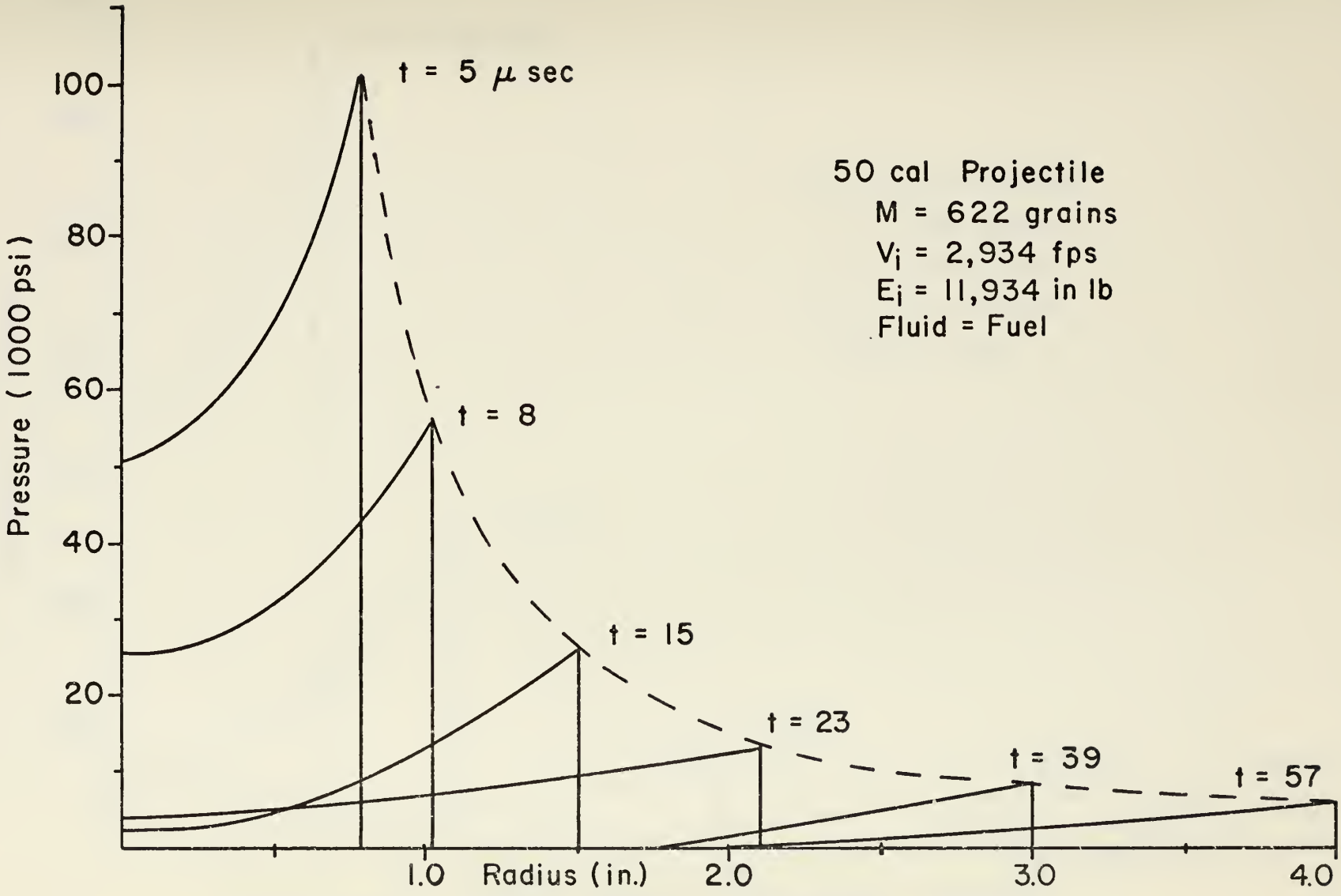

FIGURE IV-3. SHOCK PHASE PRESSURE PROFILE

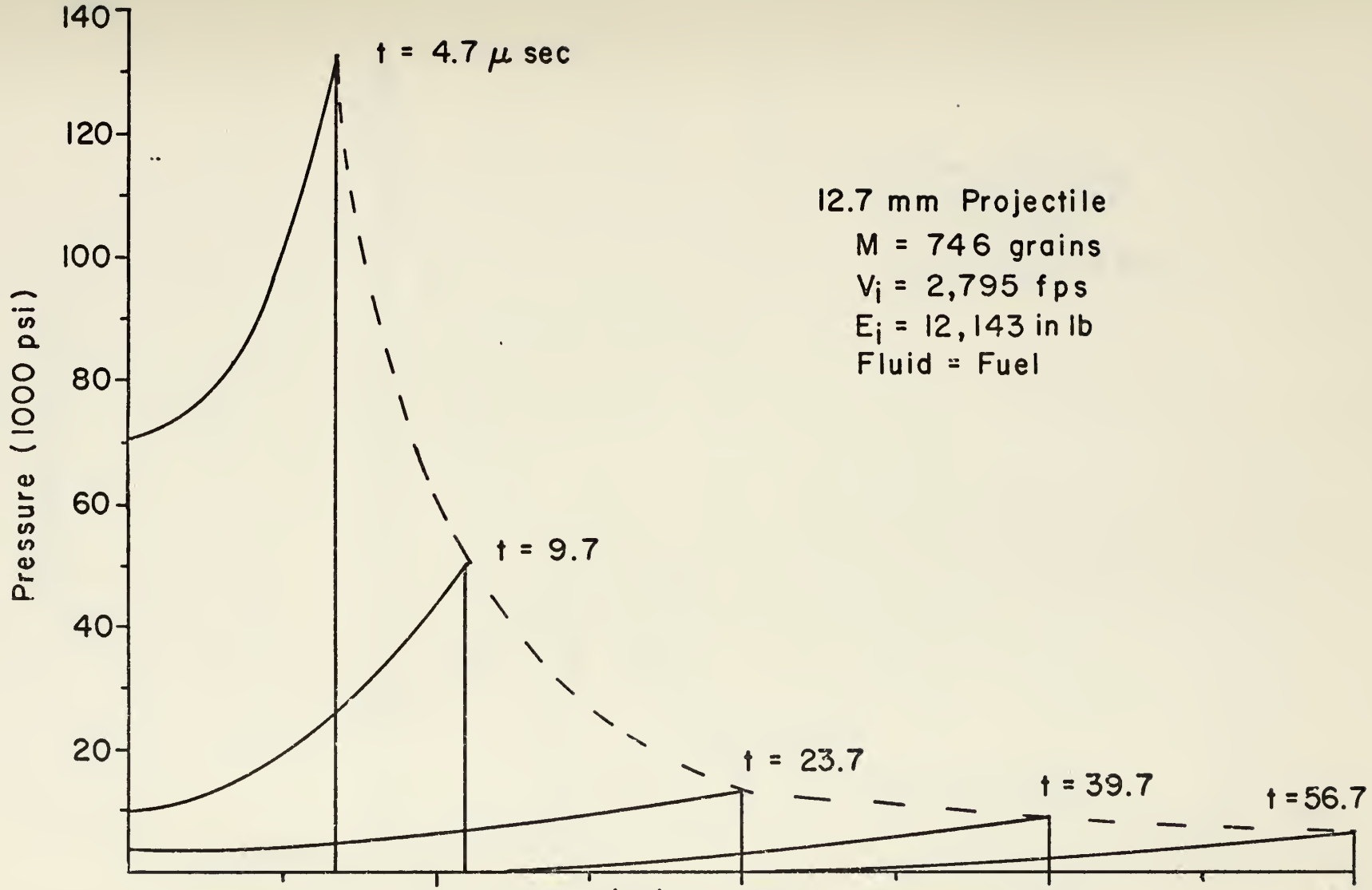

FIGURE IV-4. SHOCK PHASE PRESSURE PROFILE

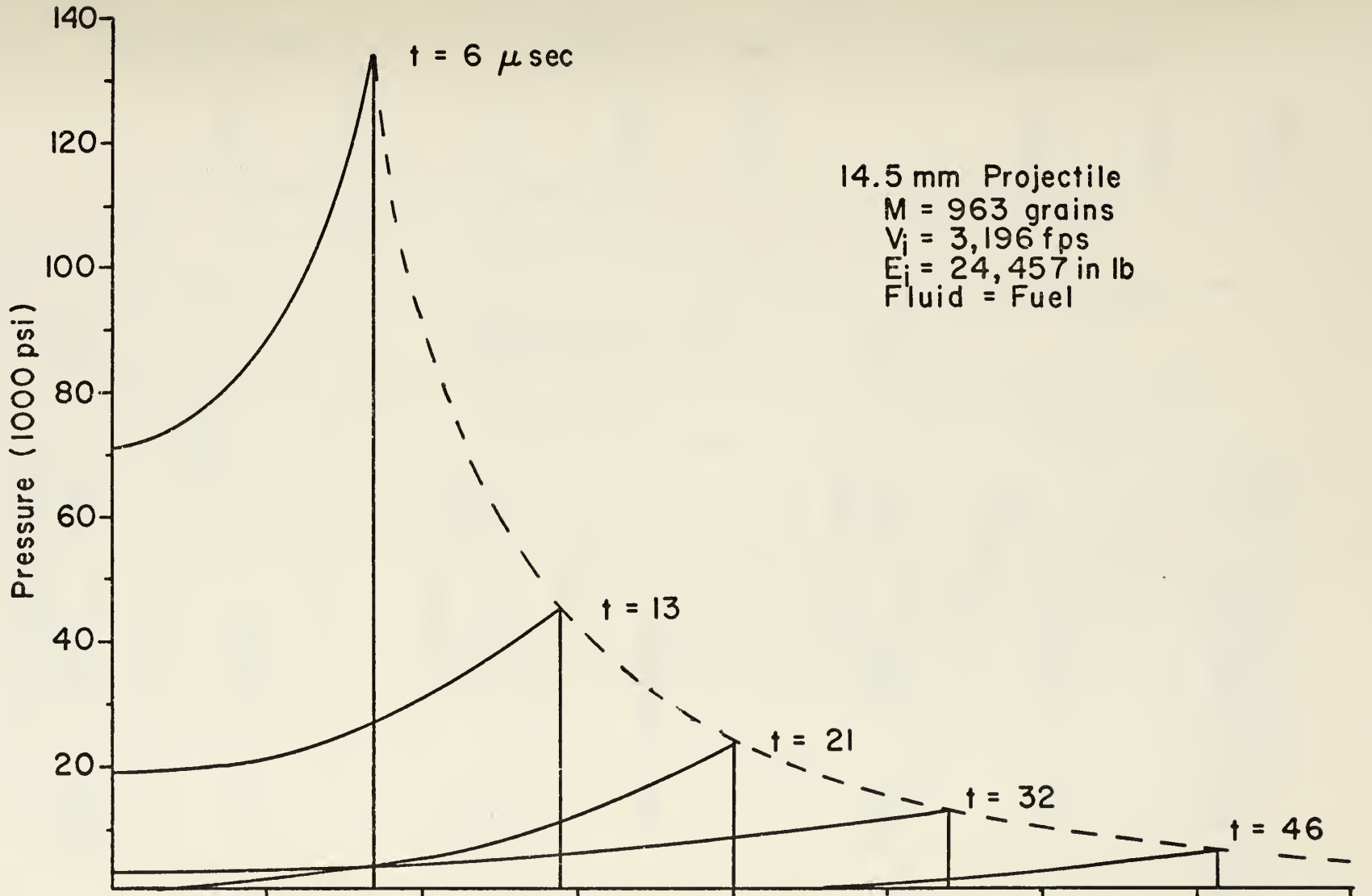

FIGURE IV-5. SHOCK PHASE PRESSURE PROFILE

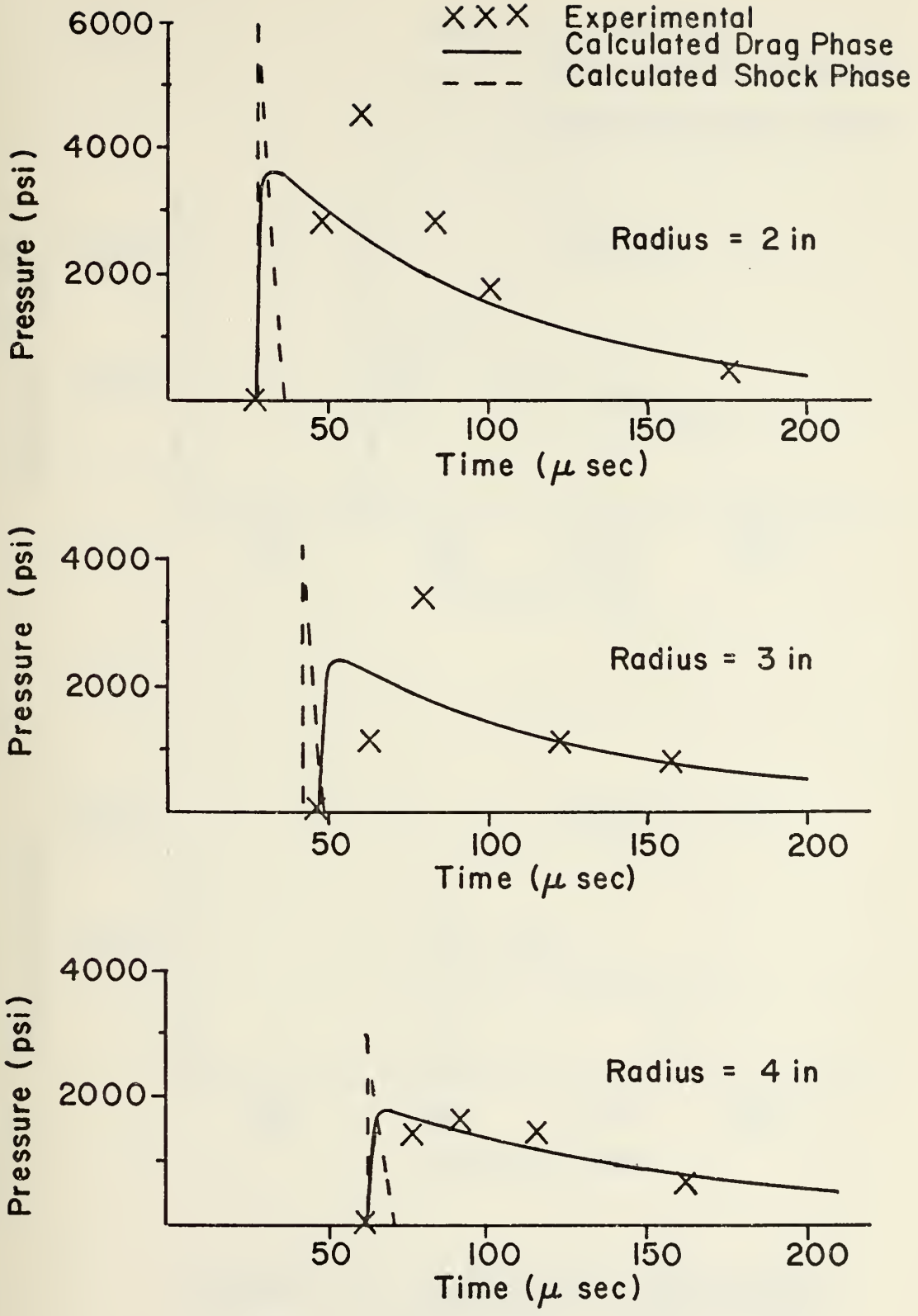

FIGURE IV-6. PRESSURE COMPARISON
E_0 = 12,323 IN. LB., HEAVY WALL

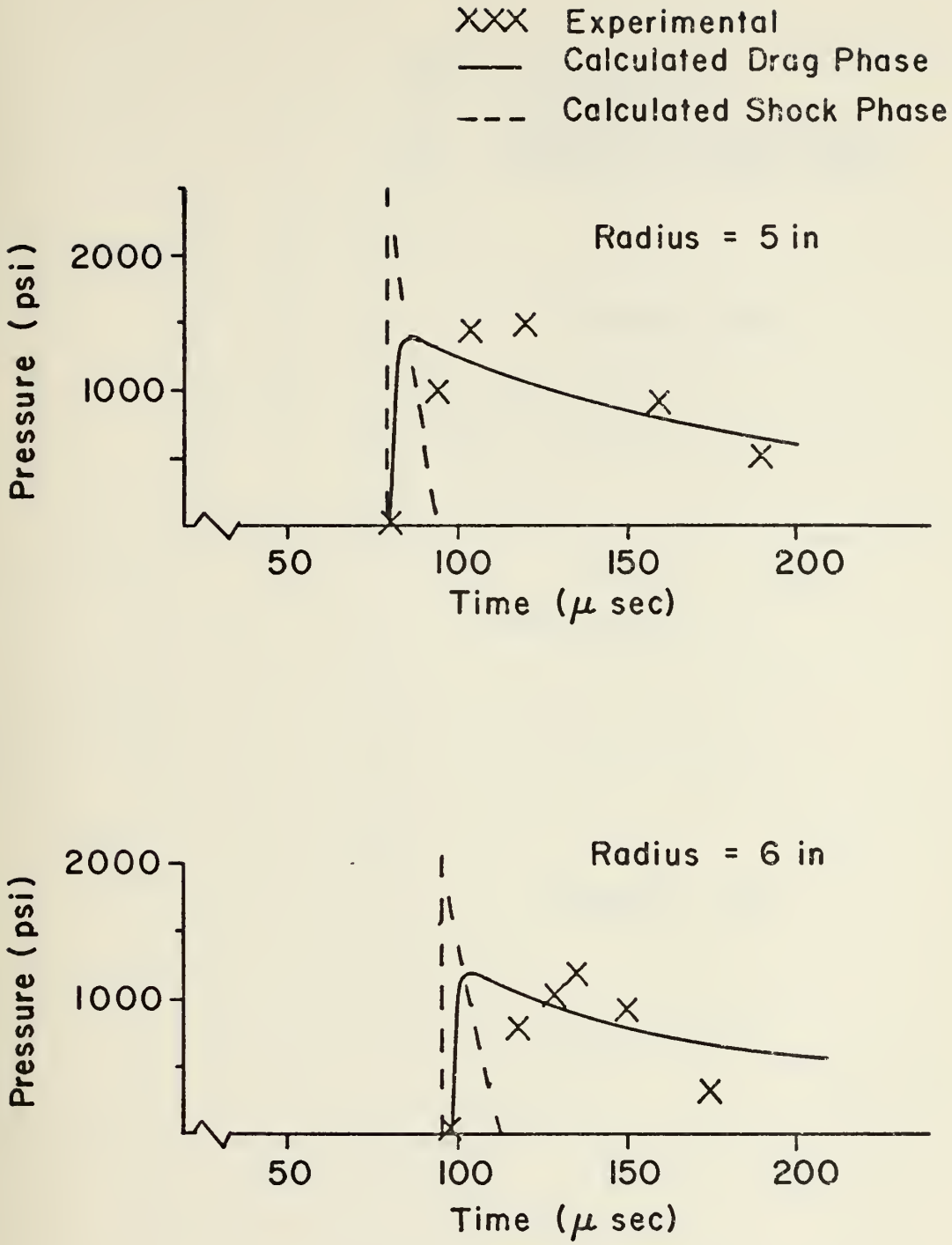

FIGURE IV-7. PRESSURE COMPARISON
E_o = 12,323 IN. LB., HEAVY WALL

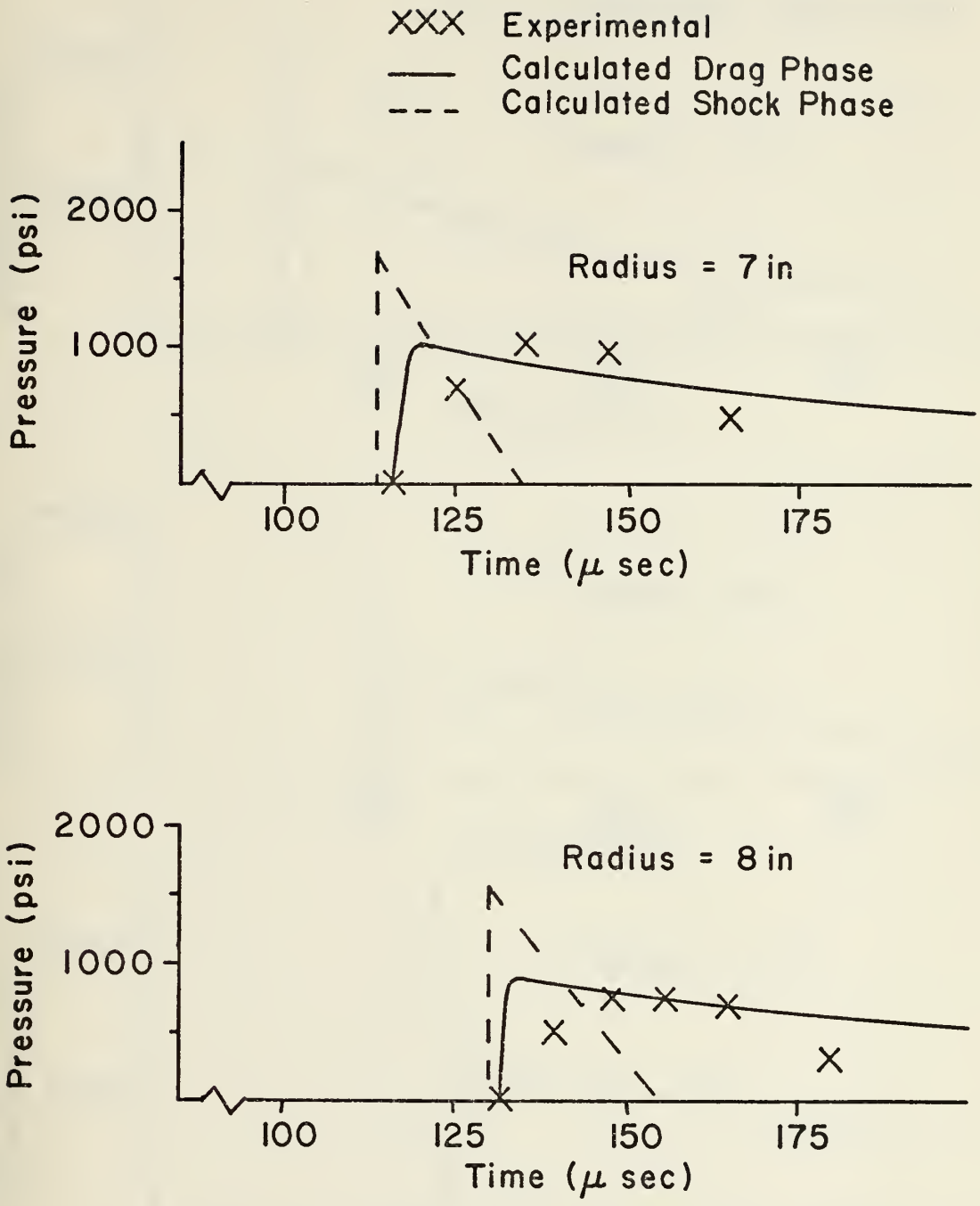

FIGURE IV-8. PRESSURE COMPARISON
E_o = 12,323 IN.LB., HEAVY WALL

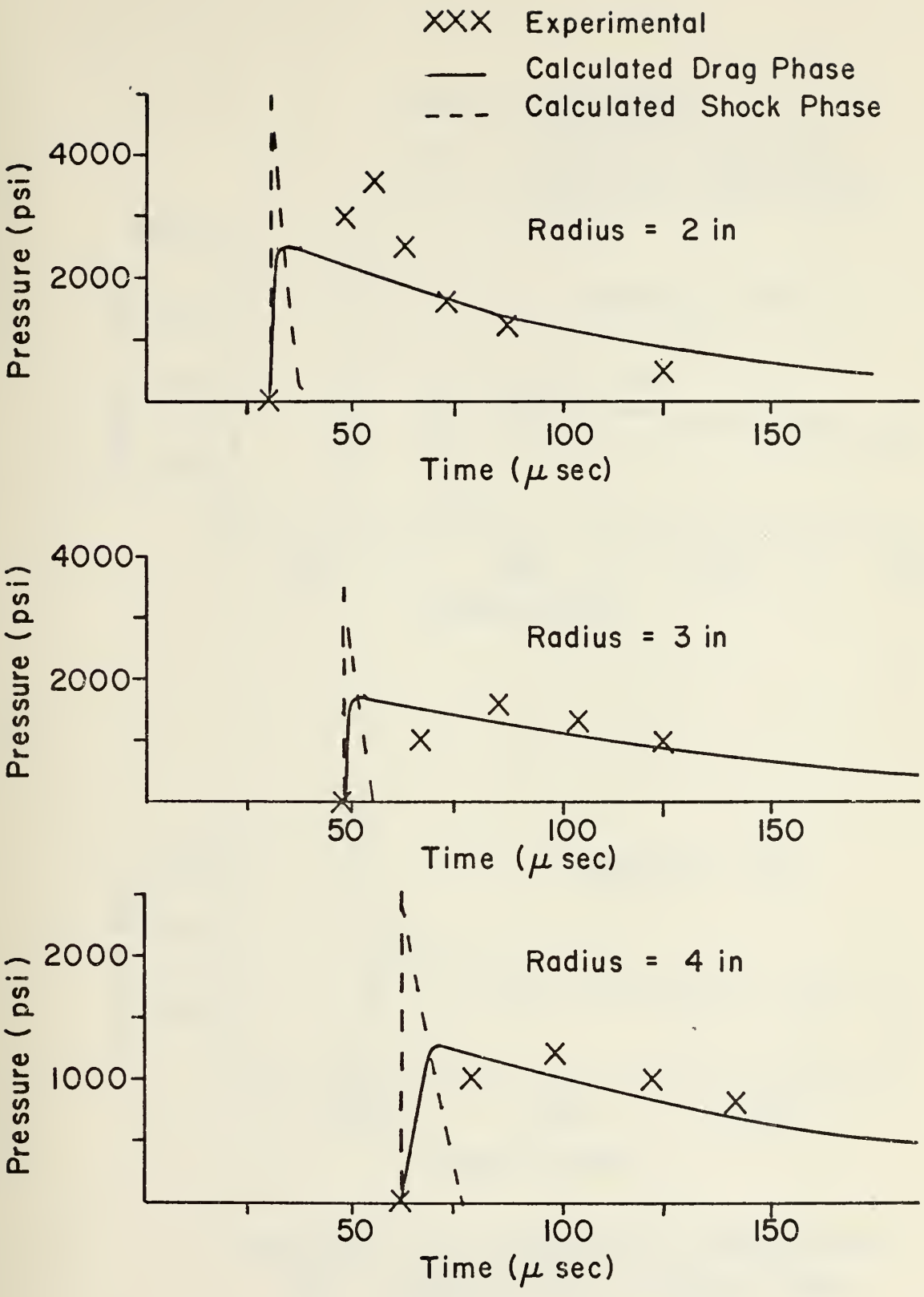

FIGURE IV-9. PRESSURE COMPARISON
E_0 = 7,493 IN. LB., HEAVY WALL

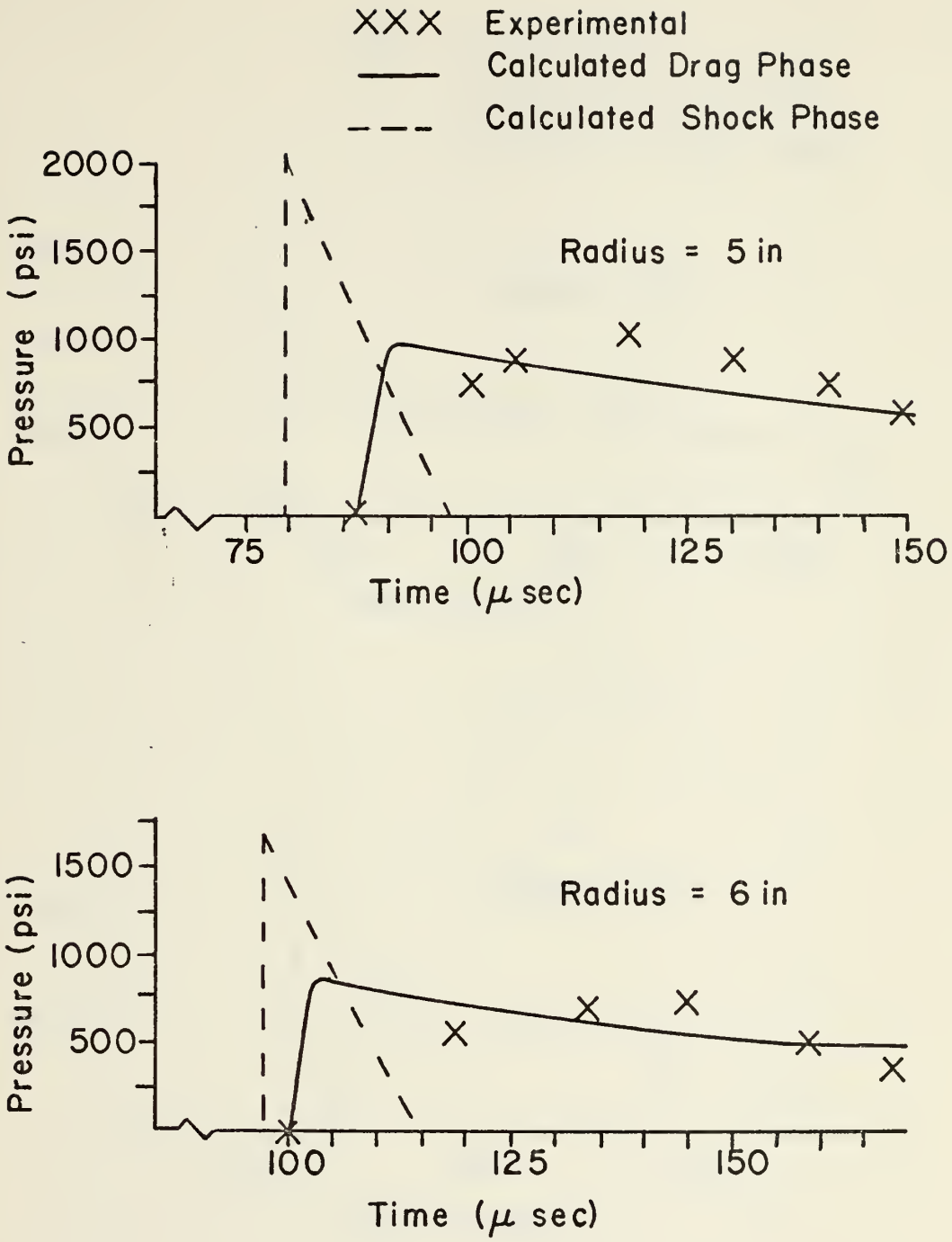

FIGURE IV-10. PRESSURE COMPARISON
E_o = 7,493 IN. LB., HEAVY WALL

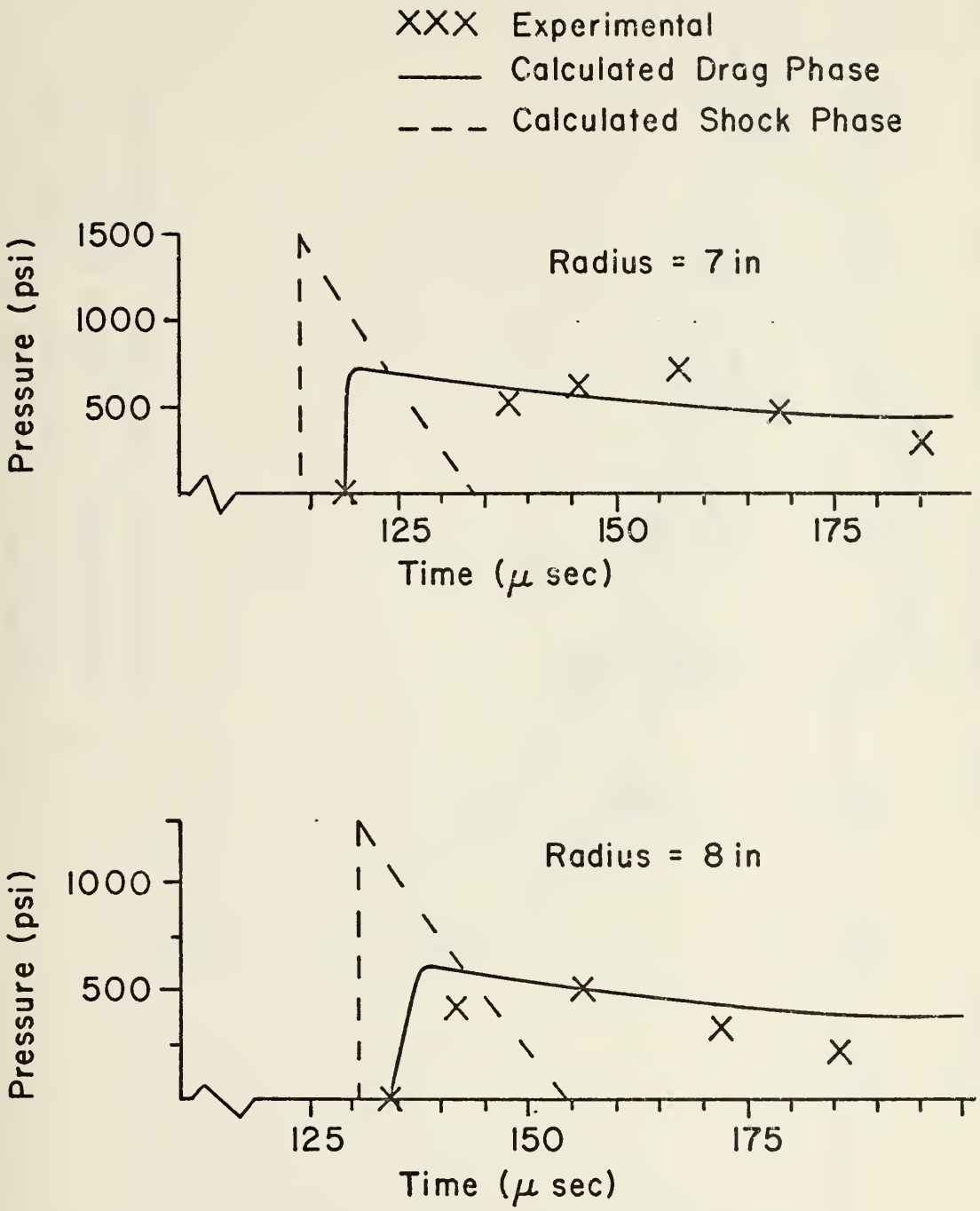

FIGURE IV-11 PRESSURE COMPARISON
E_o = 7,493 IN. LB., HEAVY WALL

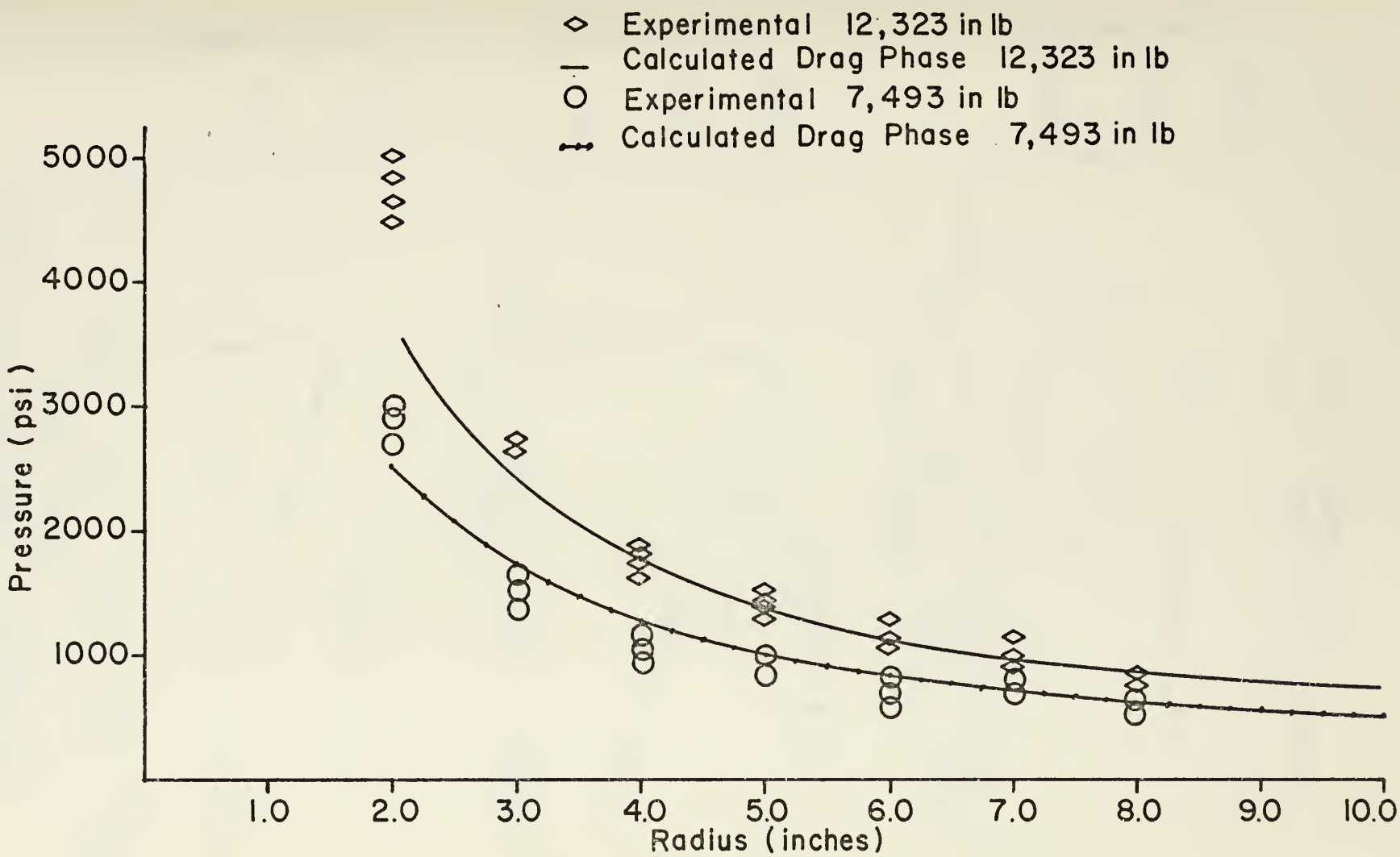

FIGURE IV-12. PEAK PRESSURE vs. RADIUS FOR HEAVY WALL

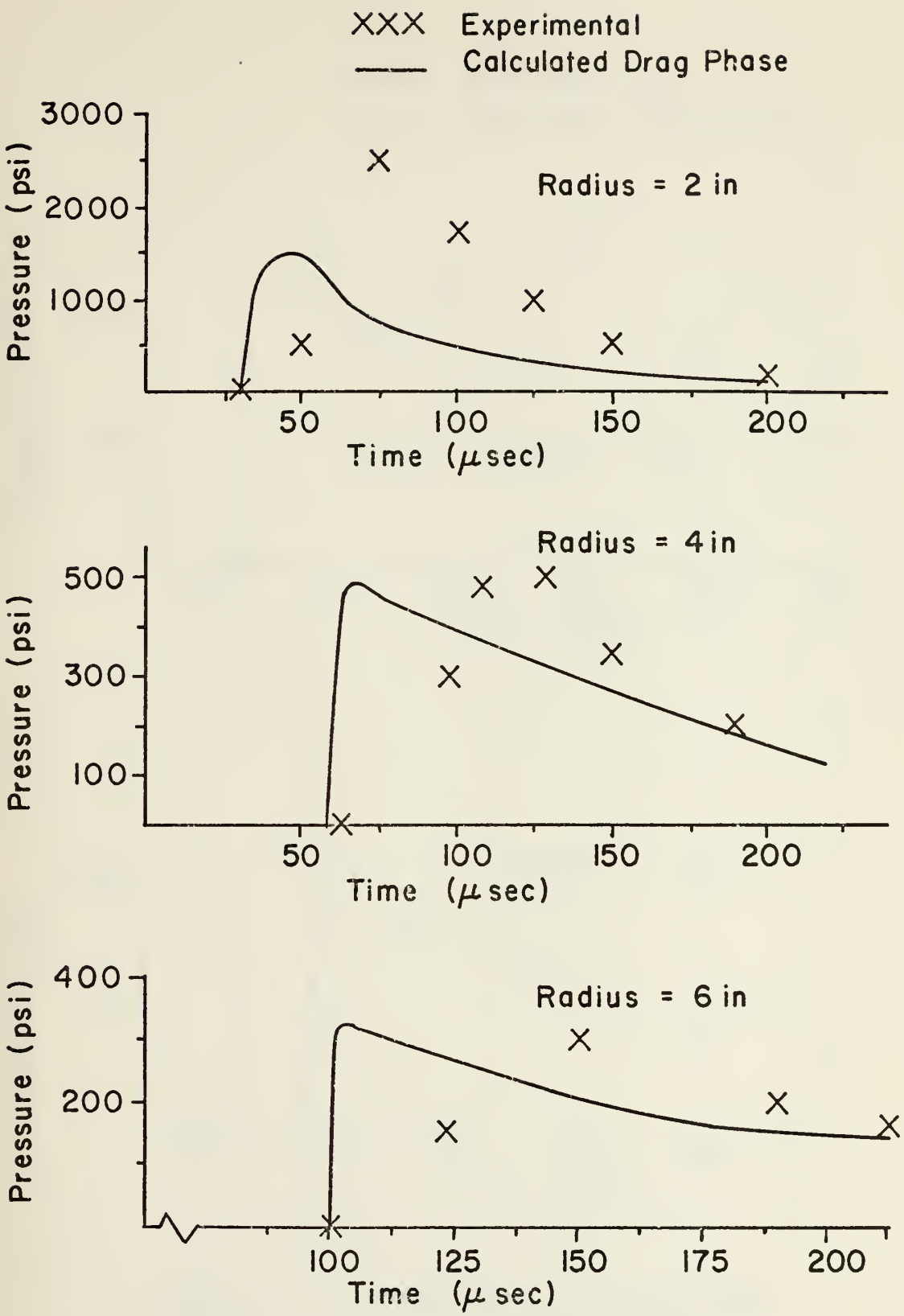

FIGURE IV-13 PRESSURE COMPARISON
E_o = 7,493 IN. LB., LIGHT WALL

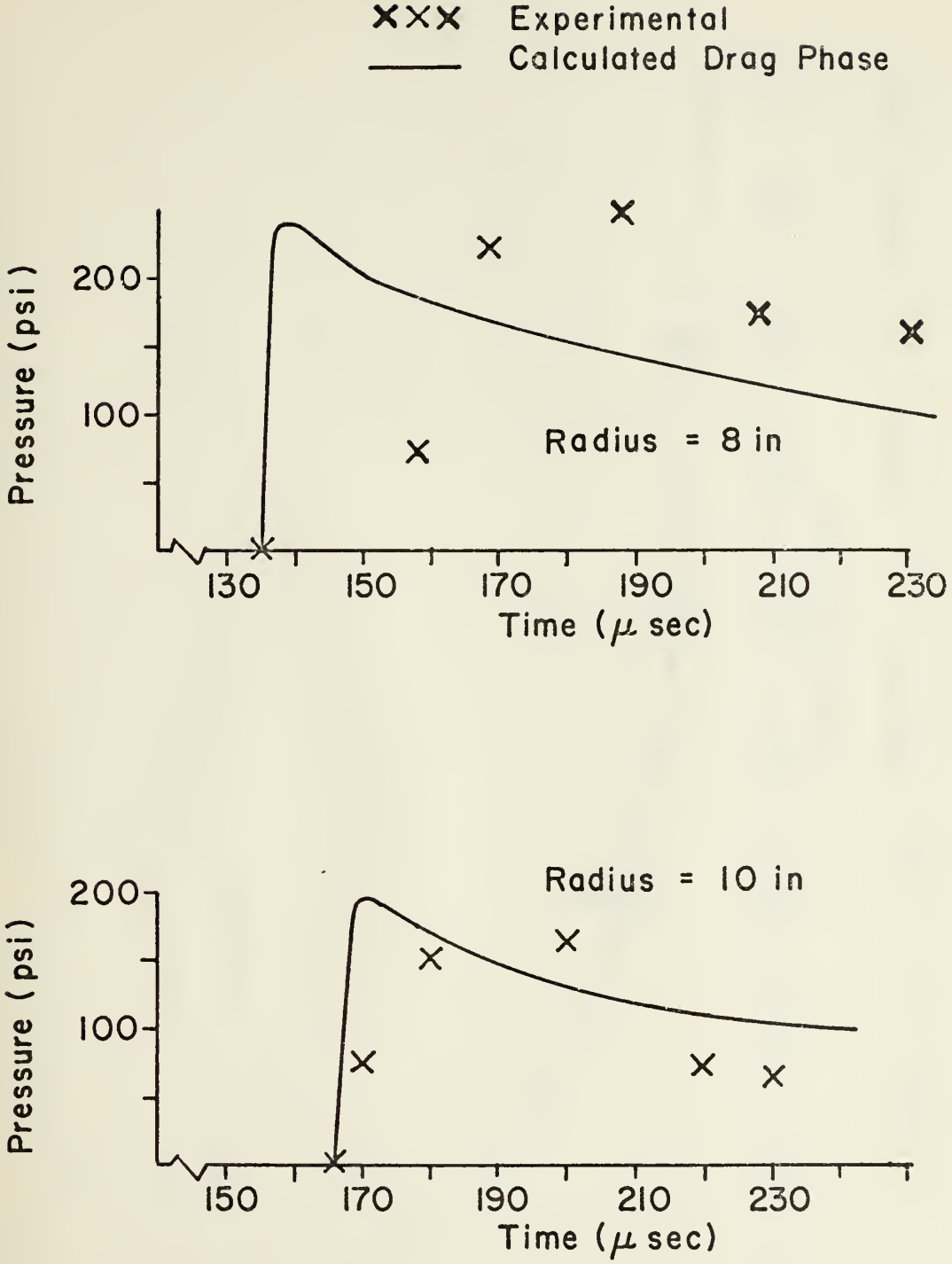

FIGURE IV-14 PRESSURE COMPARISON
E_o = 7,493 IN.LB., LIGHT WALL

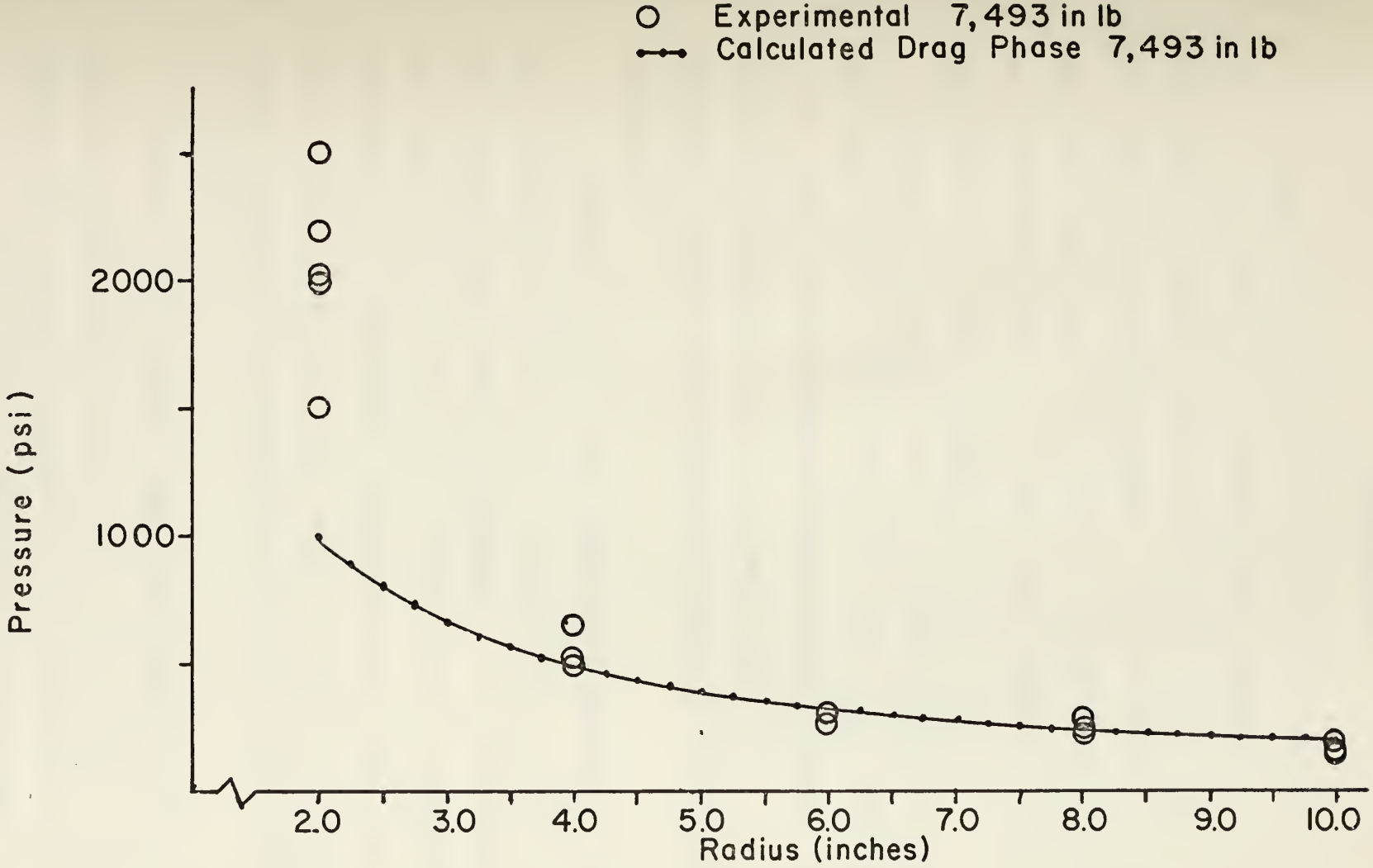

FIGURE IV-15. PEAK PRESSURE vs. RADIUS FOR LIGHT WALL

V. CONCLUSIONS

The first purpose of this study was to extend the computer code solution for shock phase pressures. This was accomplished by adding solutions for the entry phase and for the shock phase energy release. The attached code computes the shock phase pressures based on a knowledge of bullet impact parameters only. It will also compute the shock phase pressures for a point explosion in the fluid.

Attempts to verify the shock phase pressures experimentally were unsuccessful. This was due to the inadequate response time of the pressure measuring equipment. Until pressure transducers with extremely rapid rise times are available, shock phase pressures cannot be experimentally determined.

The second part of this study experimentally confirmed the analytical solution for the pressures produced in the drag phase, postulated by Lundstrom. In accomplishing this, the importance of entry wall reflections on tank internal pressures was confirmed. By using both a heavy and light wall in the experiment, and matching these with appropriate image sources in the analytical solution, the pressures were correlated.

The use of a constant drag coefficient in the analytical solution does distort the pressure wave shape. This is because the use of a constant drag coefficient is not consistent with the tumbling behavior of the bullet. At

smaller radii the experimental pressures are higher than predicted. This is due to the interaction of the shock phase pressures with the drag phase. That is, the pressure transducers are partially responding to the impulsive pressure of the shock phase.

The results of this study show that the first three phases of hydraulic ram are clearly understood and can be predicted analytically. This should be of some assistance to those responsible for increasing the survivability of aircraft subject to light or moderate damage.

```
C  ***********************************************************
C  *                                                         *
C  *                                                         *
C  *  THIS PROGRAM CALCULATES THE FOLLOWING                  *
C  *      PART I                                             *
C  *         1. SHOCK RADIUS VERSUS TIME                     *
C  *         2. SHOCK MACH NUMBER VERSUS TIME                *
C  *      PART II                                            *
C  *         1. PRESSURE VERSUS TIME AND RADIUS              *
C  *            FROM IMPACT BEHIND THE SHOCK                 *
C  *            FOR A GIVEN FLUID AND IMPACT ENERGY.         *
C  *  THIS PROGRAM ASSUMES: SHOCK RADIUS IS PROPORTIONAL TO  *
C  *  TIME TO THE 0.9 POWER UNTIL ACOUSTIC, A POWER LAW      *
C  *  DENSITY PROFILE BEHIND THE SHOCK, A STRONG SHOCK,      *
C  *  ADIABATIC ACROSS THE SHOCK, THE UNDISTURBED FLUID      *
C  *  PRESSURE IS ESSENTIALLY ZERO, SPECIFIC INTERNAL        *
C  *  ENERGY IN UNDISTURBED FLUID IS ESSENTIALLY ZERO.       *
C  *                                                         *
C  *                                                         *
C  ***********************************************************
C
C
C
C     SYMBOL DESIGNATION
C          WB=BULLET WEIGHT (GRAINS)
C          CO= SPEED OF SOUND FOR FLUID (FPS)
C          RHOO= DENSITY IN UNDISTURBED FLUID (LB/FT3)
C          VI=BULLET INITIAL VELOCITY (FPS)
C          DC= INCREMENT OF NON-DIMENSIONAL RADIUS, DELTA
C              ZHETA
C          DELT= INCREMENT OF TIME (SECS)
C          SIGMA= YIELD STRESS OF WALL (PSI)
C          RBUL=BULLET RADIUS(IN)
C          THIK=ENTRY WALL THICKNESS (IN)
C          XN=EXPONENT IN STATE EQUATION (7 FOR WATER, 10.6
C             FOR FUEL)
C          IFLAG=ZERO FOR A HEMISPHERICAL CASE.  IFLAG=ONE
C                FOR A SPHERICAL CASE.
C          TMAX=MAX TIME FOR CALCULATION OF SHOCK PRESSURES
C               (MIRCO SECONDS)
C          EO3=ENERGY RELEASE FOR SPHERICAL EXPLOSIN (INLBS)
C          EOI=IMPACT ENERGY (IN-LB)
C          EO=ENERGY GIVEN UP IN SHOCK PHASE (IN-LB)
C          X= PERCENT EO LOST AT ENTRY WALL
C          XX=PERCENT OF IMPACT ENERGY LOST IN SHOCK PHASE
C          VS= SHOCK MACH NO.
C          ET= ENERGY/VOL. = 2*EO/(R**3)
C          F1= NON-DIMENSIONAL PRESSURE AT THE SHOCK FRONT.
C              SHOCK MACH NO.
C          DODM= DERIVATIVE OF NON-DIMENSIONAL PARTICLE
C              VELOCITY W.R.T. SHOCK MACH NO. VS SHOCK
C              MACH NO.
C          XXM=INITIAL MACH NUMBER OF BULLET WITH RESPECT TO
C              FLUID (VI/CO)
      DIMENSION          PSI1(20),F1(20),VS(20), DODM(20)
     1,RXMS(20),DRS(20),ARMS(20),DT(20),T(20),RE(20),
     1RV(20),RDOD(20),XMS(20),RS(20),RPSI(20),RF(20)
      DIMENSION  TT(300),XM(300), R(300),F2(300),PSI2(300),
     1DODM2(300),Q(300),C(100),F(2,20),P(3,20)
      DIMENSION CONRS(300),SHOCV(300),TOFOR(300)
      DIMENSION FOR(20),XX(100),XXM(100)
      COMMON BQ
      DO 500 J=1,20
      FOR(J)=0.0
  500 CONTINUE
      N=19
      READ (5,100) WB,CO,RHOO,VI,DC,DELT,SIGMA,RBUL,THIK,XN
      READ (5,203) IFLAG,TMAX,EO3
```

```
      READ (5,101)(VS(I) , I=1,N )
      READ(5,101)(XX(I),I=1,32)
      READ(5,101)(XXM(I),I=1,32)
      WRITE (6,200) WB,CO,RHOO,VI,DC,DELT,SIGMA,RBUL,THIK,XN
      WRITE (6,204) IFLAG,TMAX
      DO 15 I=1,N
   15 WRITE(6,202) VS(I)
      DO 16 I=1,32
   16 WRITE(6,201) XX(I),XXM(I)
C
C     PART I
C     PERCENTAGE OF INITIAL ENERGY DEPOSITED AND INITIAL
C     SHOCK RADIUS
C
      EOI=WB*1.4286*12.*VI*VI/(64.4*10.**4.)
      X=1. -(SIGMA*THIK*3.1416*RBUL*RBUL/EOI )
      EO=X*EOI
C          CALCULATION OF ENERGY GIVEN UP IN SHOCK PHASE
      IF (IFLAG.GT.0) GO TO 3
      XBM=VI/CO
      XE=PIF2(XBM,XXM,32,XX)
      EO=XE*EO
      GO TO 4
    3 EO=EO3
    4 RO=(EO*32.2*144./(RHOO*CO*CO*2.*3.1416))**0.33333
C
C     INITIAL VALUE OF ENERGY/VOL.
C
      ETO=2.*EO/(RO**3.0)
C
C     INTEGRATE ENERGY EQUATION TO FIND SHOCK MACH #,
C     DENSITY AND PRESSURE RATIO.
C
      CALL ENERG (IFLAG,ETO,CO,RHOO,XN,VMS,PSI10,F10)
      VSO=VMS
      VSI=0.01
      CALL DEVF1 (VSO,VSI,XN,DODMO)
C
C     COMPUTE INITIAL TIME FOR DISTANCE RO
C
      TO=RO/(CO*VSO*12.0)
C
C     ASSIGN SUBSEQUENT VALUES OF SHOCK MACH NO. AT WHICH
C     SHOCK RADIUS WILL BE COMPUTED
C
      DO 10  I=1,N
      IF (VSO-VS(I))  1,2,2
    1 GO TO 10
    2 M=N-I+1
      XMS(1)=VSO
      GO TO 11
   10 CONTINUE
C
C     COMPUTE SUBSEQUENT VALUES OF SHOCK RADIUS
C
   11 RS(1)=RO
      DO 20  J=2,M
      XMS(J)=VS(I)
      VSE=XMS(J)
      CALL SUBEN (IFLAG,CO,RHOO,XN,VSE,ET)
      RS(J)=(2.*EO/(ET))**0.3333
      I=I+1
   20 CONTINUE
      K=M-1
C
C     COMPUTE DELTA TIME CORRESPONDING TO SHOCK MACH NO.
C     AND SHOCK RADIUS
C
      DO 30  I=1,K
      DRS(I)= RS(I+1)-RS(I)
      ARMS(I)=2./(XMS(I)+XMS(I+1))
   30 DT(I)=DRS(I)*ARMS(I)/(CO*12.0)
```

```
      T(1)=T0
      DO  40  J=2,M
   40 T(J)= T(J-1)+DT(J-1)
      IF(RHOO.LT.60.0) WRITE(6,104)
      IF(RHOO.GT.61.0) WRITE(6,102)
      WRITE (6,103)  E0
      WRITE (6,110)
C
C     PRINT SHOCK MACH NO. AND SHOCK RADIUS VS TIME
C
      DO 50  I=1,M
   50 WRITE (6,111)  T(I),XMS(I),RS(I)
  100 FORMAT  (8E10.0)
  101 FORMAT  (8E10.0)
  102 FORMAT (1H,//,39X,'ENERGY',15X,'FLUID WATER')
  103 FORMAT (29X,1E20.7)
  104 FORMAT(1H,//,39X,'ENERGY',15X,'FLUID FUEL')
  110 FORMAT (1H,//,39X 'TIME',17X,'MACH',17X,'RADIUS' )
  111 FORMAT  (29X,3E20.7)
  200 FORMAT (//10E12.5//)
  201 FORMAT (15X,2E20.7)
  202 FORMAT(15X,1E20.7)
  203 FORMAT (I2,2E10.0)
  204 FORMAT (//10XI2,20XE12.5//)
C
C
C     PART II
C
C
C     INITIALIZE VARIABLES AND ASSIGN VALUES USED WITH
C     NON-DIMENSIONAL PRESSURE DISTRIBUTION FUNCTION
C
      BBB=T(M)*1.E06+1.05
      L=BBB
      TT(1)=0.0
      XM(1)=XMS(1)
      R(1)=R0
      F2(1)=F10
      PSI2(1)=PSI10
      DODM2(1)=DODM0
      Q(1)=3.*(PSI10-1.0)
      B=-0.25
      I=1.0/DC +1.05
      C(1)=0.0
      WRITE (6,301)
      WRITE (6,302) TT(1),XM(1),R(1)
      WRITE (6,303)
      DO 60   J=2,N
   60 C(J)=C(J-1)+DC
C
C     COMPUTE NON-DIMENSIONAL AND DIMENSIONAL PRESSURE FOR
C     INITIAL SHOCK RADIUS.
C
      DO 70 J=1,I
      F(1,J)=F2(1)+PSI2(1)*(C(J)**(Q(1)+2.0)-1.0)*(F2(1)/
     1PSI2(1)-B*(F2(1)+XM(1)*DODM2(1)))/(Q(1)+2.0)
      P(1,J)=F(1,J)*RHOO*CO*CO*XM(1)*XM(1)/(32.2*144.)
   70 CONTINUE
      K=1
      JJ=1
      SUM=0.0
      CALL FORCE(FOR,C,P,R,I,JJ,K)
      DO 501 J=1,I
      SUM=SUM+FOR(J)
      WRITE(6,304) C(J),P(1,J),F(1,J),FOR(J)
  501 CONTINUE
      TOFOR(1)=SUM
C
C     ITERATION TO SOLVE PRESSURE, SHOCK RADIUS, SHOCK MACH
C     NO. VS TIME
C
      DO 80   K=2,L
```

```
      TT(K)=TT(K-1)+DELT
      IF (TT(K)-TO)   21,21,22
   21 XM(K)=XM(1)
      R(K)=R(1)
      F2(K)=F2(1)
      PSI2(K)=PSI2(1)
      DODM2(K)=DODM2(1)
      Q(K)= Q(1)
      DO 55  J=1,I
   55 P(2,J)=P(1,J)
      GO TO 80
   22 X=TT(K)
C
C     INTERPOLATION OF INPUT DATA AND PART I DATA FOR
C     VARIABLES IN PRESSURE FUNCTION
C
      XM(K)=PIF2(X,T,M,XMS)
      R(K)=PIF2(X,T,M,RS)
      VSS=XM(K)
      CALL SHOCK (XN,VSS,PSI3,F12)
      PSI2(K)=PSI3
      F2(K)=F12
      CALL DEVF1 (VSS,VSI,XN,DODM3)
      DODM2(K)=DODM3
      Q(K)=3.*(PSI2(K)-1.0)
      WRITE  (6,301)
      WRITE  (6,302) TT(K),XM(K),R(K)
      WRITE  (6,303)
      DO 90  J=1,I
      F(2,J)=F2(K)+PSI2(K)*(C(J)**(Q(K)+2.0)-1.0)*(F2(K)/
     1PSI2(K)-B*(F2(K)+XM(K)*DODM2(K)))/(Q(K)+2.0)
      P(2,J)=F(2,J)*RHOO*CO*CO*XM(K)*XM(K)/(32.2*144.)
   90 CONTINUE
      JJ=2
      SUM=0.0
      CALL FORCE(FOR,C,P,R,I,JJ,K)
      DO 502 J=1,I
      SUM=SUM+FOR(J)
      WRITE(6,304) C(J),P(2,J),F(2,J),FOR(J)
  502 CONTINUE
      TOFOR(K)=SUM
   80 CONTINUE
C
C     ACOUSTIC EXTENSION OF THE MACH WAVE.
C
      KK=TMAX+1.05
      LL=L+1
      DO 610 K=LL,KK
      TT(K)=TT(K-1)+DELT
      XM(K)=1.00
      R(K)=R(K-1)+CO*DELT*12.0
      WRITE (6,301)
      WRITE (6,302) TT(K),XM(K),R(K)
      WRITE (6,303)
      DO 600 J=1,I
      P(3,J)=F(2,J)*RHOO*CO*CO/(32.2*144.*R(K))
  600 WRITE (6,306) C(J),P(3,J),F(2,J)
  610 CONTINUE
      WRITE(6,305)
      CALL CONVER(R,XM,TOFOR,TT,L)
   91 FORMAT (3E15.5)
   92 FORMAT (1E15.5)
  301 FORMAT (1H,//,36X,'TIME',17X,'MACH',17X,'RADIUS' )
  302 FORMAT (29X,3E20.7)
  303 FORMAT(1H,//,39X,'R/RS',17X,'P',17X,'F',19X,'FORCE')
  304 FORMAT(29X,4E20.7)
  305 FORMAT(1H,//,36X,'TIME',17X,'VELO',17X,'RADUIS',17X,'T
     1OFORCE')
  306 FORMAT (29X,3E20.7)
      END
```

```
      FUNCTION PIF2 (X,XLIST,N,FLIST)
C
CC    SECOND ORDER INTERPOLATION
C
      DIMENSION XLIST (100), FLIST (100)
      BLIF (P,Q,R,S,T) = ((Q-P)*(S-T)/(R-Q)+S)
      IF (X-XLIST(N)) 2,1,1
    1 I = N-1
      GO TO 5
    2 IF(X-XLIST(1)) 4,4,6
    4 I = 1
    5 K = 1
      GO TO 30
    6 K = 2
    7 DO 8 I = 1,N
      IF (X-XLIST(I)) 9,9,8
    8 CONTINUE
      I=N
    9 I = I-1
   30 BLIF1 = BLIF(X,XLIST(I),XLIST(I+1),FLIST(I),FLIST(I+1)
     1)
   10 IF (K-1) 11,11,12
   11 PIF2 = BLIF1
      RETURN
   12 IF((I+2)-N) 13,13,16
   13 IF ((I-1)-1) 15,14,14
   14 IF(ABS(XLIST(I-1)-X)-ABS(XLIST(I+2)-X))16,15,15
   15 L = I+2
      GO TO 17
   16 L = I-1
   17 BLIF2 = BLIF (X,XLIST(I),XLIST(L),FLIST(I),FLIST(L))
      PIF2 = BLIF (X,XLIST(I+1),XLIST(L),BLIF1,BLIF2)
   18 RETURN
      END


      SUBROUTINE FORCE(FOR,C,P,R,I,JJ,K)
C
CC    THIS SUBROUTINE COMPUTES THE FORCE ON THE ENTRY WALL
CC    DUE TO SHOCK PHASE FOR A FRONT WALL WITH A
CC    PRE-PUNCHED HOLE.
CC    RHRS= NON-DIMENSIONAL RADIUS OF PRE-PUNCHED HOLE
CC    S= SLOPE OF STRAIGHT LINE BETWEEN PRESSURE DATA
CC         POINTS
CC    RX= THE INTERCEPT OF R/RS,NON-DIMENSIONAL RADIUS,
CC        WHERE PRESSURE IS ZERO
CC    FOR(N)= FORCE(LB) FOR AN ANNULUS WHOSE OUTSIDE RADIUS
CC            IS C(N) AND INSIDE RADIUS IS C(N-1)
CC
C
      DIMENSION FOR(20),C(100),P(2,20),R(300)
      RHRS=.375/R(K)
      IF(RHRS-1.) 100,25,25
  100 IF(JJ-1) 1,1,2
    1 DO 10 N=2,I
      S=(P(1,N)-P(1,N-1))*4.
      IF(P(1,N-1)) 3,4,4
    3 IF(P(1,N)) 5,5,6
    5 FOR(N)=0.0
      GO TO 10
    6 RX=(S*C(N-1)-P(1,N-1))/S
      IF(RHRS.GT.C(N)) GO TO 43
      IF(RX.GT.RHRS) GO TO 60
      PH=S*(RHRS-C(N-1))+P(1,N-1)
      FOR(N)=(.5*(P(1,N)-PH)+PH)*3.1416*(C(N)*C(N)-RHRS
     1*RHRS)*R(K)*R(K)
      GO TO 10
   60 FOR(N)=P(1,N)*.5*3.1416*(C(N)*C(N)-RX*RX)*R(K)*R(K)
      GO TO 10
    4 IF(RHRS-C(N-1)) 40,40,41
   40 FOR(N)=(.5*(P(1,N)-P(1,N-1))+P(1,N-1))*3.1416*(C(N)
     1*C(N)-C(N-1)*C(N-1))*R(K)*R(K)
```

```
      GO TO 10
   41 IF(RHRS-C(N)) 42,43,43
   42 PH=S*(RHRS-C(N-1))+P(1,N-1)
      FOR(N)=(.5*(P(1,N)-PH)+PH)*3.1416*(C(N)*C(N)-RHRS
     1*RHRS)*R(K)*R(K)
      GO TO 10
   43 FOR(N)=0.0
   10 CONTINUE
      RETURN
    2 DO 20 N=2,I
      S=(P(2,N)-P(2,N-1))*4.
      IF(P(2,N-1)) 13,14,14
   13 IF(P(2,N)) 15,15,16
   15 FOR(N)=0.0
      GO TO 20
   16 RX=(S*C(N-1)-P(2,N-1))/S
      IF(RHRS.GT.C(N)) GO TO 143
      IF(RX.GT.RHRS) GO TO 160
      PH=S*(RHRS-C(N-1))+P(2,N-1)
      FOR(N)=(.5*(P(2,N)-PH)+PH)*3.1416*(C(N)*C(N)-RHRS
     1*RHRS)*R(K)*R(K)
      GO TO 20
  160 FOR(N)=P(2,N)*.5*3.1416*(C(N)*C(N)-RX*RX)*R(K)*R(K)
      GO TO 20
   14 IF(RHRS-C(N-1)) 140,140,141
  140 FOR(N)=(.5*(P(2,N)-P(2,N-1))+P(2,N-1))*3.1416*(C(N)
     1*C(N)-C(N-1)*C(N-1))*R(K)*R(K)
      GO TO 20
  141 IF(RHRS-C(N)) 142,143,143
  142 PH=S*(RHRS-C(N-1))+P(2,N-1)
      FOR(N)=(.5*(P(2,N)-PH)+PH)*3.1416*(C(N)*C(N)-RHRS
     1*RHRS)*R(K)*R(K)
      GO TO 20
  143 FOR(N)=0.0
   20 CONTINUE
   25 RETURN
      END


      SUBROUTINE CONVER(R,XM,TOFOR,TT,L)
C
C     THIS SUBROUTINE CONVERTS VELOCITY AND RADIUS
C     TO KM/SEC AND CM RESPECTIVELY
C
      DIMENSION R(300),XM(300),TOFOR(300),CONRS(300),SHOCV(
     1300),TT(300)
      DO 510 II=1,L
      CONRS(II)=R(II)*2.54
      SHOCV(II)=XM(II)*4.9/3.281
      WRITE(6,520) TT(II),SHOCV(II),CONRS(II),TOFOR(II)
  520 FORMAT(29X,4E20.7)
  510 CONTINUE
      RETURN
      END


      SUBROUTINE SHOCK(XN,VS,PSI1,F1)
C
C     THIS SUBROUTINE COMPUTES THE NON-DIMENSIONAL PRESSURE
C     AND DENSITY AT THE SHOCK FRONT.
C
      F(X)=-X+1/(1-B*(X**XN-1))
      X1=(XN*(VS**2.))**(1/XN)-0.05
      B=1/(XN*(VS**2.))
    5 DO 10 I=1,200
      X1=X1-0.005
      IF(X1.LT.0.0) GO TO 20
      Y=F(X1)
      IF(Y.LE.0.001) GO TO 40
   10 CONTINUE
   20 DO 30 J=1,200
      X1=X1+0.0025
```

```
      IF(X1.GT.0.0) GO TO 5
      Y=F(X1)
      IF(Y.LE.0.001) GO TO 40
   30 CONTINUE
   40 PSI1=X1
      F1=((PSI1**XN)-1.)/(XN*(VS**2.))
      RETURN
      END


      SUBROUTINE DEVF1(VS,VSI,XN,DODM)
C
C     THIS SUBROUTINE COMPUTES THE DERIVATIVE OF THE
C     NON-DIMENSIONAL PARTICLE VELOCITY WITH RESPECT TO THE
C     SHOCK MACH NUMBER.
C
      VSA=VS+VSI
      VSB=VS-VSI
      CALL SHOCK(XN,VSA,PSIA,FA)
      CALL SHOCK(XN,VSB,PSIB,FB)
      DODM=(FA-FB)/(2.*VSI)
      RETURN
      END


      SUBROUTINE ENERG (IFLAG,ETO,CO,RHOO,XN,VMS,PSI10,F10)
C
C     THIS SUBROUTINE COMPUTES THE INITIAL SHOCK MACH NUMBER
C     BY INTEGRATION OF THE ENERGY EQUATION.  THE EXTERNAL
C     SUBROUTINE QG10 IS A GUASSIAN 10 POINT QUADRATURE.
C
      EXTERNAL FCT
      COMMON BQ
      C=2.0
      IF(IFLAG.EQ.0) C=1.0
      VSG=4.0
      CALL SHOCK (XN,VSG,PSI10,F10)
      A=3.1416*(RHOO/32.2)*(CO*CO/144.0)*(VSG**2.0)*PSI10
     1*F10*F10*2.0
      BQ=3.*PSI10-1.
      CALL QG10 (0.0,1.0,FCT,EP)
      ETG=A*EP*C
      IF(ETO-ETG) 40,100,50
   40 VSG=VSG-.1
      CALL SHOCK (XN,VSG,PSI10,F10)
      BQ=3.*PSI10-1.
      CALL QG10 (0.0,1.0,FCT,EP)
      ETG=A*EP*C
      IF(ETG-ETO) 60,100,40
   60 VSG=VSG+.001
      CALL SHOCK (XN,VSG,PSI10,F10)
      A=3.1416*(RHOO/32.2)*(CO*CO/144.0)*(VSG**2.0)*PSI10
     1*F10*F10*2.0
      BQ=3.*PSI10-1.
      CALL QG10 (0.0,1.0,FCT,EP)
      ETG=A*EP*C
      IF(ETG-ETO) 60,100,100
   50 VSG=VSG+.1
      CALL SHOCK (XN,VSG,PSI10,F10)
      A=3.1416*(RHOO/32.2)*(CO*CO/144.0)*(VSG**2.0)*PSI10
     1*F10*F10*2.0
      BQ=3.*PSI10-1.
      CALL QG10 (0.0,1.0,FCT,EP)
      ETG=A*EP*C
      IF(ETG-ETO) 50,100,90
   90 VSG=VSG-.001
      CALL SHOCK (XN,VSG,PSI10,F10)
      A=3.1416*(RHOO/32.2)*(CO*CO/144.0)*(VSG**2.0)*PSI10
     1*F10*F10*2.0
      BQ=3.*PSI10-1.
      CALL QG10 (0.0,1.0,FCT,EP)
      ETG=A*EP*C
```

```
      IF(ETG-ET0) 100,100,90
  100 VMS=VSG
      RETURN
      END


      SUBROUTINE SUBEN(IFLAG,C0,RHO0,XN,VSE,ET)
C
C     THIS SUBROUTINE COMPUTES THE ENERGY BEHIND THE SHOCK
C     FRONT FOR A GIVEN MACH NO.  THE EXTERNAL INTEGRATION
C     SUBROUTINE QG10 IS A GAUSSIAN 10 POINT QUADRATURE.
C
      EXTERNAL FCT
      COMMON BQ
      C=2.0
      IF(IFLAG.EQ.0) C=1.0
      CALL SHOCK (XN,VSE,PSIE,FE)
      A=3.1416*(RHO0/32.2)*(C0*C0/144.0)*(VSE**2.0)*PSIE
     1*FE*FE*2.0
      BQ=3.*PSIE-1.
      CALL QG10 (0.0,1.0,FCT,EE)
      ET=A*EE*C
      RETURN
      END


      FUNCTION FCT(X)
C
C     THIS FUNCTION SUBPROGRAM GENERATES FUNCTIONS FOR THE
C     INTEGRATION ROUTINES.
C
      COMMON BQ
      FCT=(1.+X**2.)*X**BQ
      RETURN
      END
```

LIST OF REFERENCES

1. McDonnel Aircraft Engineering Methods Authorization, F65-76-555, Hydraulic Ram: A Fuel Tank Vulnerability Study, by R. N. Yurkovich, September 1969.

2. Naval Weapons Center Technical Publication, 5227, Fluid Dynamic Analysis of Hydraulic Ram, by E. A. Lundstrom, July 1971.

3. Soper, W.R., Hydraulic Ram Studies, MSAE Thesis, Naval Postgraduate School, Monterey, California, December 1973.

4. Kappel, L.S., Hydraulic Ram Shock Phase Effects on Fuel Cell Survivability, MSAE Thesis, Naval Postgraduate School, Monterey, California, March 1974.

5. NASA Technical Note, NASA TN D-3143, Investigation of Characteristics of Pressure Waves Generated in Water Filled Tanks Impacted by High Velocity Projectiles, by F. S. Stepka, C. R. Morse, and R. P. Dengler, December 1965.

6. McMillen, J. Howard, "Shock Wave Pressures in Water Produced by Impact of Small Spheres," Physical Review, v. 68, pp. 198-208, 1 November 1945.

7. Naval Weapons Center Film 6HR1-7, Hydraulic Ram Exit Wall Test, February 1974.

8. Power, H.L., "FY 75 Experimental Hydraulic Ram Studies," NPS-57Ph74081, June 1975.

9. Holm, C.M., Hydraulic Ram Pressure Measurements, MSAE Thesis, Naval Postgraduate School, Monterey, California, December 1974.

10. Douglas Aircraft Company Contract N00019-69-G-0181, Fuel Tank Vulnerability Reduction, by H. F. Winchester, J. F. Denlinger, G. A. Vickers, W. R. Dunbar, and L. D. Christensen, April 1970.

11. Joint Technical Coordinating Group, Aircraft Survivability Report 74-7-015, Fluid Dynamic Analysis of Hydraulic Ram III, by E. A. Lundstrom and W. K. Fund, October 1974.

INITIAL DISTRIBUTION LIST

		No. Copies
1.	Defense Documentation Center Cameron Station Alexandria, Virginia 22314	2
2.	Library, Code 0212 Naval Postgraduate School Monterey, California 93940	2
3.	Chairman, Department of Aeronautics, Code 57 Naval Postgraduate School Monterey, California 93940	1
4.	Professor H. L. Power, Jr., Code 57Ph Department of Aeronautics Naval Postgraduate School Monterey, California 93940	1
5.	Professor R. E. Ball, Code 57Ba Department of Aeronautics Naval Postgraduate School Monterey, California 93940	1
6.	Mr. Wallace K. Fung, Code 5114 Naval Weapons Center China Lake, California 93555	20
7.	LCDR John W. Patterson #3 Pinehill Way Monterey, California 93940	2